CONTINUOUS CHARACTERIZATION OF UNIVERSAL INVERTIBLE AMPLIFIER USING SOURCE NOISE

A Thesis

Submitted to the Faculty

of

Purdue University

by

Chandrama Ahmed

In Partial Fulfillment of the

Requirements for the Degree

of

Master of Science in Biomedical Engineering

December 2017

Purdue University

Indianapolis, Indiana

THE PURDUE UNIVERSITY GRADUATE SCHOOL
STATEMENT OF COMMITTEE APPROVAL

Dr. Ken Yoshida, Chair

Department of Biomedical Engineering

Dr. Edward J. Berbari

Department of Biomedical Engineering

Dr. Paul Salama

Department of Electrical and Computer Engineering

Approved by:

Dr. Julie Ji

Head of the Graduate Program

ACKNOWLEDGMENTS

I would like to first thank my family for all the sacrifices they have made. I never had so much faith in myself that they have always had in me.

I am grateful to Dr. Ken Yoshida for giving me the opportunity of working in Bioelectronics lab and guiding me throughout this project while I repeatedly lost hopes. The countless 'I have an idea, let's try it this way...' in the face of repeated failures taught me I can never give up.

I would also like to thank my academic committee members Dr. Edward Berbari and Dr. Paul Salama for helping me with the many problems I faced during the different stages of this project.

Working in this lab taught me it is, if not impossible, very difficult to solve any problem with individual effort. Thanks to Mike Bertram, Ryne Horn and Namrata Temghare for their contributions in this project. Many thanks to all my lab members, past and present, for their supports and encouragements throughout the years.

I would also like to thank Sherry Clemens. While being absorbed with the many problems in the lab, I have regretfully developed a habit of messing up the deadline for administrative paperworks and every time Sherry has appeared as a life saver.

And thanks to NIH and R2i for funding my education and the project.

TABLE OF CONTENTS

Page

LIST OF FIGURES

Figure Page

Figure Page

LIST OF SYMBOLS

V	Voltage
μV	microvolt
Ω	Ohm
$\hat{\mathbf{x}}$	signal estimate
$\mathbf{P}$	estimation error
$\mathbf{x}$	internal state of the system
$\mathbf{A}$	State transformation Matrix
$\mathbf{B}$	Input Coupling Matrix
$\mathbf{C}$	Output Coupling Matrix
$\mathbf{D}$	Feedthrough Matrix
$\mathbf{Q}$	system covariance
$\mathbf{R}$	measurement covariance
$\mathbf{K}$	Kalman gain
TF	System Transfer Function
TFest	Estimated Transfer Function

LIST OF ABBREVIATIONS

UIA	Universal Invertible Amplifier
KVL	Kirchoff's Voltage Law
DC	Direct Current
RMS	Root Mean Squared
SNR	Signal-to-Noise Ratio
TF	Transfer Function
KHz	Kilohertz
EIP	Electrode Interface Potential
ECG	Electrocardiogram
EMG	Electromyogram
ENG	Electroneuralgram
IACUC	Institution of Animal Care and Use Committee
TIME	Transverse Intrafascicular Multichannel Electrode

ABSTRACT

Ahmed, Chandrama M.S.B.M.E., Purdue University, December 2017. Continuous Characterization of Universal Invertible Amplifier Using Source Noise. Major Professor: Ken Yoshida.

With passage of time and repeated usage of a system, component values that make up the system parameters change, causing errors in its functional output. In order to ensure the fidelity of the results derived from these systems it is thus very important to keep track of the system parameters while being used. This thesis introduces a method for tracking the existing system parameters while the system was being used using the inherent noise of its signal source. Kalman filter algorithm is used to track the inherent noise response to the system and use that response to estimate the system parameters. In this thesis this continuous characterization scheme has been used on a Universal Invertible Amplifier (UIA).

Current biomedical research as well as diagnostic medicine depend a lot on shape profile of bio-electric signals of different sources, for example heart, muscle, nerve, brain etc. making it very important to capture the different event of these signals without the distortion usually introduced by the filtering of the amplifier system. The Universal Invertible Amplifier extracts the original signal in electrodes by inverting the filtered and compressed signal while its gain bandwidth profile allows it to capture from the entire bandwidth of bioelectric signals.

For this inversion to be successful the captured compressed and filtered signals needs to be inverted with the actual system parameters that the system had during capturing the signals, not its original parameters. The continuous characterization scheme introduced in this thesis is aimed at knowing the system parameters of the

UIA by tracking the response of its source noise and estimating its transfer function from that.

Two types of source noises have been tried out in this method, an externally added noise that was digitally generated and a noise that inherently contaminates the signals the system is trying to capture. In our cases, the UIA was used to capture nerve activity from vagus nerve where the signal was contaminated with electrocardiogram signals providing us with a well-defined inherent noise whose response could be tracked with Kalman Filter and used to estimate the transfer function of UIA.

The transfer function estimation using the externally added noise did not produce good results but could be improved by means that can be explored as future direction of this project. However continuous characterization using the inherent noise, a bioelectric signal, was successful producing transfer function estimates with minimal error. Thus this thesis was successful to introduce a novel approach for system characterization using bio-signal contamination.

1. INTRODUCTION

Todays diagnostic medicine relies heavily on the bio-electric signals originating from bio-electric activities of different tissues, which imposes utmost importance on measurement fidelity. The instrumentation for processing and recording each of the different signals including electrocardiogram (ECG), electromyogram (EMG), Electroneurogram (ENG) etc. have evolved based on the unique characteristics of the respective signal, becoming highly specialized and unsuitable for use with a different bio-signal. Approaches are being made to design systems that address the need for a universal system capable of capturing the varying wide spectrum of bioelectric signals.

Design of all these specialized as well as universal systems comes down to the simple electric components like resistors and capacitors. With advanced technology in play it is possible to have very high precision components. These nonetheless will either have some degrees of variance in their value or drift from their original values with time or both, affecting the performance of the system and the signal they are used to capture. While it is vastly beneficial to have a universal system capable of capturing different bio-signals, it is of paramount importance to have a knowledge of the fidelity of the system as well as the captured signal.

This thesis stems from these two needs: a functional universal system compatible with the wide range of bio-signal spectrum and a use-case characterization schema for the system that ensures its stability and the fidelity of any signal it is responsible to process. Here use-case characterization can be defined as obtaining the parameter values that the system had while being used as opposed to real-time characterization which is obtaining them during its use.

The basis of the first need, design of a successful universal system for processing bio-signals has been addressed in a previous work [1] on which this thesis introduces some improvements. The second need, design of a schema for use-case characterization of a system uses Kalman filter, an estimation algorithm, to track the system transfer function.

Background for both the needs is described in this introduction while details on the design and procedure are described in the subsequent chapters.

1.1 Prior Works of This Thesis: An Introduction to Universal Invertible Amplifier

Current technologies available for recording or monitoring bio-signals focus on specific signals with distinct set of system parameters. Thus multiple number of systems are required for recording different signals. A convenient solution would be design of an analog system versatile enough to be able to capture bio-signals from different sources and digitally robust enough that the different signals can be extracted from the captured mixed signal in digital end processing. Universal Invertible Amplifier, UIA is an amplifier that uses a compressor-expander architecture employing a variable gain tuned to the bandwidth characteristics of bio-signals.

The common amplifier filtering systems used in recording the different biosignals additionally distort the signal in order to reduce noise and to elevate Signal-to-Noise ratio (SNR) within the frequency bandwidth of signal of interest. However this filtering causes irreversible distortion, making it impossible to go back to the original signal that is seen at the electrode even during post processing. The filtering along with attenuating the noise affects the shape of the signal of interest to some extent making a shape dependent detection or diagnosis difficult. Thus it is necessary to go back to the original signal seen at the electrode for shape based detection of signal of interest [1].

Inspired from the need of such a common convergent system with a reversible filtering architecture a first order UIA was built successfully [2]. However the very small scale neural signal prompted the necessity for a higher gain system, hence a second order UIA was designed with a similar basic principle as the first one but with a better system characterization schema because a higher order system is more susceptible to instability and signal infidelity.

1.1.1 Universal Invertible Amplifier Architecture

Universal Invertible Amplifier, UIA architecture involves an analog front end which is the compressor and a digital back end that is the expander. The basic principle for the compressor is a variable gain amplification and filtering strategy that spans the entire spectrum of bioelectric signals. This has been possible because the general bioelectric signal profile follows a low pass filter characteristics as shown in Figure 1.1. Thus the compressor follows a high pass filter profile to counter balance the bioelectric profile. This serves the purpose of increasing the resolution with which the compressed signal can be captured.

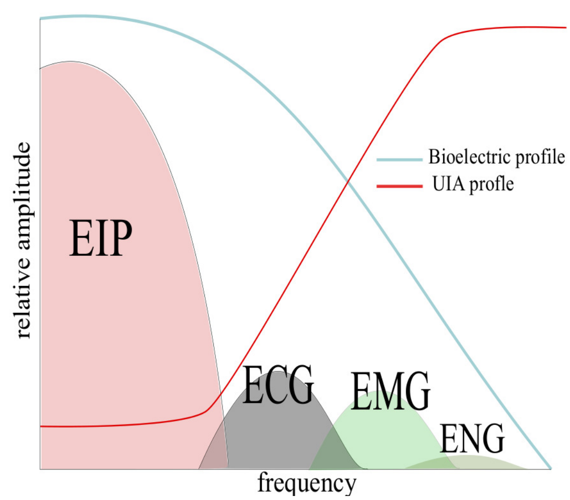

Fig. 1.1.: UIA profile (red) counter balancing general bioelectric signal profile (blue). In general bio-electric signals fit into low-pass filter characteristics thus, making UIA profile a high-pass filter with defined gain at low frequency range. This is adopted from [1].

Across the entire spectrum different bio-signals show different magnitude profile, with Electrode Interface Potential, EIP, having magnitudes in the range of V and Electromyogram, EMG and Electroneurogram, ENG in the range of mV and μV [3] spanning a high range of magnitude. The amplifier captures the signals in the low frequency region, that inherently have comparatively larger amplitude with a lower gain profile whereas, in the high frequency region where the signals generally have a comparatively lower amplitude the amplifier captures with a higher gain profile. Hence, at the output the entire bio spectrum is captured at same magnitude scales. On the recording side the entire resolution available for recording can be employed within this shorter range of magnitudes enabling very high resolution recording. This schema of compressing the signal based on its magnitude and then expanding later is not new, the principle of companding system was first patented by AT&T [4] and then it had been used by the music industry.

The compressor consists of a flat low gain stage that captures the DC parts of the bio-spectrum and a main amplifier with the mentioned high pass filter profile that keeps the entire amplifier from saturating [1]. The entire architecture is described in the thesis works done by Kevin Mauser [1].

The digital back end or the expander is a digital filter that employs the inverted transfer function of the UIA analog front end (1/UIA compressor transfer function) which reverses the distortion applied by the compressor and goes back to the original signal seen at the input of UIA compressor. The inverted signal should be a mixture of different bio-signals from where the signal of interest can be extracted with digitally filtering the inverted signal within the spectral band of the signal of interest.

The first generation UIA, described in [1], UIA01 Figure 1.2 is a first order amplifier-filter system with a gain profile of 2-1000, Figure 1.3 over a frequency bandwidth of DC-20 KHz. The instrumentation amplifier, INA 111 [5] at the front end acts as a high impedance headstage and provides with a variable gain of 1-500 over DC-20 KHz. The general purpose Op-amp OP27 [6] at the final stage provides with a flat gain of 2 over all the frequencies.

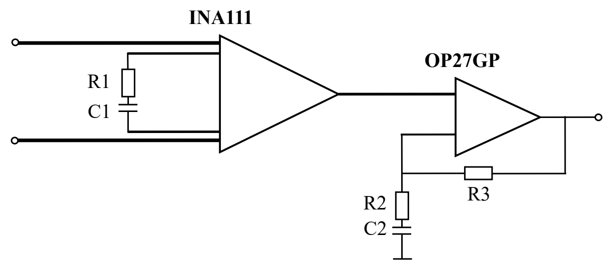

Fig. 1.2.: UIA01, first generation UIA, circuit diagram. The Instrumentation Amplifier INA111 forms the first stage and shapes the high-pass filter profile of the system. OP27GP a the final stage provides a flat gain 2 over all frequencies.

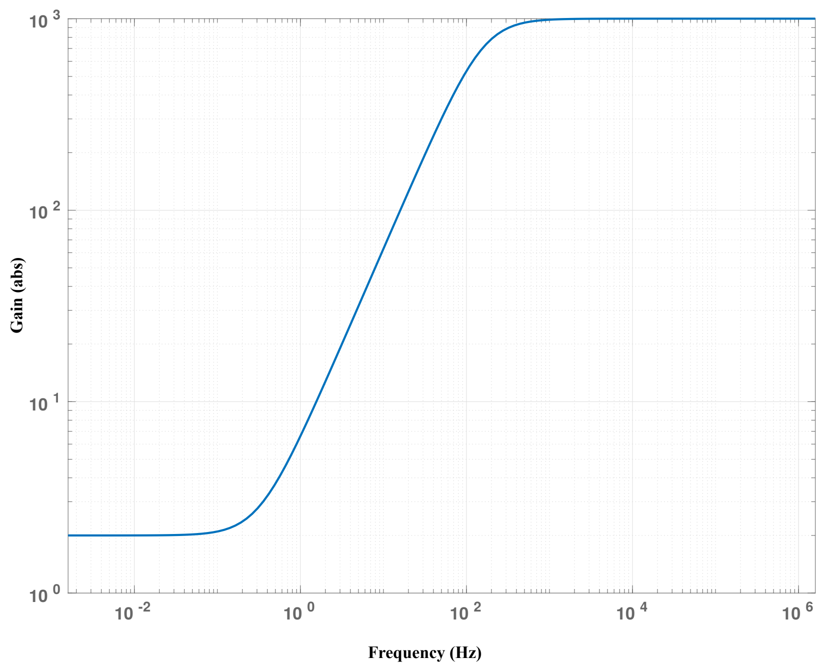

Fig. 1.3.: UIA01 frequency response. With a flat gain of 2 over the low frequency range DC-0.1Hz and of 1000 over the high frequency range beyond 1KHz it holds the variable gain region within 0.1Hz-1KHz with a first order high-pass filter profile.

The second order UIA was implemented by modifying the high pass filter in the compressor into a second order one and adding an additional channel to the input for realizing use-case characterization. The second order UIA modification and its bench-top characterization is discussed in detail in chapter 2.

1.2 Use-Case Characterization: System Parameter Estimation

The analog amplifier and filter chains used in the recording instrumentation are all comprised of passive elements such as resistors and capacitors. These passive elements tend to drift from their original values used in the design of the system depending on multiple factors like passage of time, continuous usage, temperature etc..These shifts in the original value are so small that in most applications they do not affect the results. But in the case of bio-signal processing even very small amount of shifts may be potential to cause shape distortion of the signal of interest, more so in case of neural signals, which being very small are very much susceptible to changes in the amplification system. Thus it is very important to keep track of the changes in the system parameter values to compensate for them in post-process. Many high fidelity recording systems compensates for the distortion by using the *apriori* characterization of the system, but cannot compensate for changes taking place during usage.

The Universal Invertible Amplifier (UIA) architecture involves an expander stage that inverts captured signal by the amplifier to refer to the original signal seen at the electrode. This expander is essentially the inverted transfer function of the system, which is known beforehand. But if the transfer function shifts during use because of any change in the parameter values, inversion of the captured signal by the original transfer function would cause distortion which fails the purpose of UIA. Besides, the second order UIA being a fourth order system, a second order compressor and a second order expander, its susceptibility to distortion is even more.

This thesis is inspired from the need for a continuous characterization scheme, introducing a way to track the changes in parameter values thus enabling use-case characterization of the system. The method used takes advantage of Kalman filter algorithm [7]. In this thesis, its filtering property is used but in the reverse manner, it is used to track the noise instead of tracking the actual signal for characterizing the system.

1.2.1 An Introduction to Kalman Filter

Kalman filter as an estimation algorithm has been around for more than 50 years. Introduced by Emil Rudolf Kalman in 1960 [8] it found very fast acceptance in NASA [7] and saw and continues to see extensive application in solving navigation problems in marine systems, astronomy, Global Positioning Systems (GPS) etc. [9]. Kalman filter made the application of estimation algorithm in modern control system easier and in recent times its modifications like extended Kalman filter, EKF is being used for nonlinear systems [7] . Kalman Filtering, Theory and Practices [7] by Mohinder S. Grewal and Angus P. Andrews does a great job of introducing its background history as well as the basics of its derivation. A short introduction of its working procedure will be provided here to help understand the transfer function estimation calculation.

Before diving into Kalman filter theory, however, one needs to have a basic understanding about system modeling, especially state-space modeling, which is the domain Kalman filter problems are defined in.

1.2.2 System Models

A system can be modeled in different ways, in different domains. Two such models are transfer function model and state space model. A transfer function model gives the input-output relation of a system in the frequency domain (as a function of s). A state pace model on the other hand defines the system just not by its input-output relation, rather it looks into the internal state of the system in time domain (as a function of t).

State Space Model

State space model is a time domain approach of defining a system by its inputs, outputs and the internal state variables. It is essentially breaking down and representing an Nth-order system into N first order differential equations. An analogy by

Raymond A. DeCarlo [10] explains it as adding a perspective to the system definition. An object can be seen from the top-down view or an oblique side view, Figure 1.4. The oblique side view obviously adds new information about the object which can be

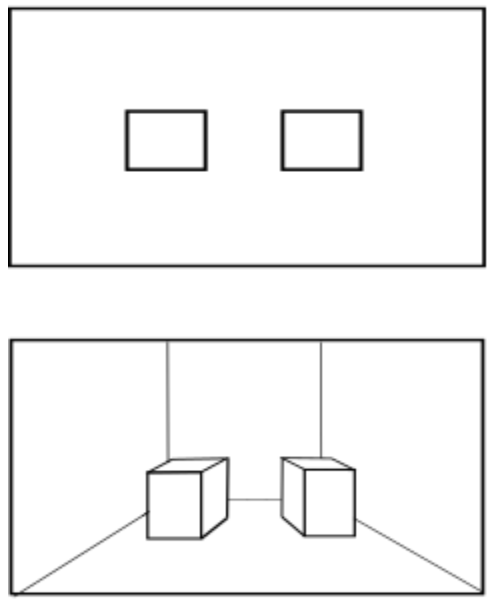

Fig. 1.4.: Top view (above) versus side-view (below) of objects, adopted from [10] . The oblique view in this case carries additional information about the dimensions.

considered as the state variables conveying information about the internal state of a system. Formally state of a system is defined as the minimum set of internal variables which if known at time t_0 is sufficient to specify the system at any time t given that the input for time t is known [10, 11].

The block diagram in Figure 1.5 shows the state space representation of a discrete system.

Here,

$\mathbf{u}_k$ = value of the input U at time point t_k

$\mathbf{y}_k$ = value of the output Y at the time point t_k

$\mathbf{x}_k$ = value of the state variable X at the time point t_k

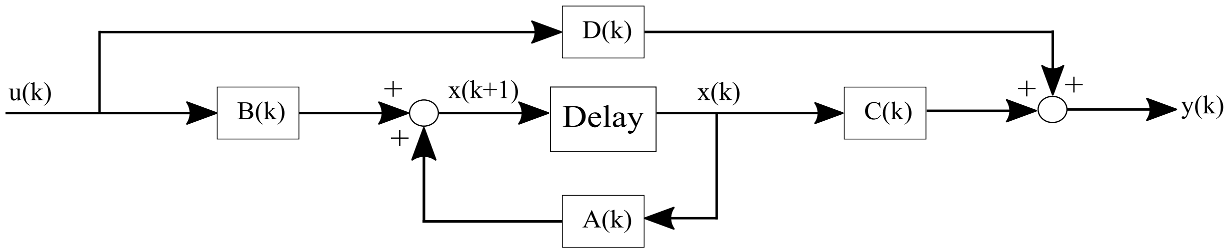

Fig. 1.5.: Block Diagram of a lumped system in state space model.

$\mathbf{x}_{k+1}$ = value of the state variable X at the next time point t_{k+1}

$\mathbf{A}_k$ = State transition matrix, that relates state variable from previous time to its state in next time point.

$\mathbf{B}_k$ = Input coupling matrix, that relates the state variable to the deterministic input

$\mathbf{C}_k$ = Output coupling matrix, translates the state variable to the output

$\mathbf{D}_k$ = Feed through matrix, relates the deterministic input to the output.

The model equations for this discrete system is given by:

$$\mathbf{x}_{k+1} = \mathbf{A}_k\mathbf{x}_k + \mathbf{B}_k\mathbf{u}_k \tag{1.1}$$

$$\mathbf{y}_k = \mathbf{C}_k\mathbf{x}_k + \mathbf{D}_k\mathbf{u}_k \tag{1.2}$$

For example, The state space model for the RC circuit in Figure 1.6 can be given by Equation 1.6.

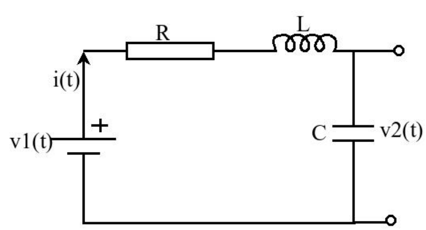

Fig. 1.6.: RLC series circuit.

Using Kirchoff's Voltage Law (KVL) in the circuit, we have,

$$\frac{d^2 v_2(t)}{dt^2} = \frac{-R}{L}\frac{dv_2}{dt} - v_2\frac{1}{LC} + v_1\frac{1}{LC} \tag{1.3}$$

With Y = $V_2(t)$, the output, we can define the state variables,

$$X1 = Y \tag{1.4}$$

$$X2 = X1 \tag{1.5}$$

Thus,

$$\dot{X}1 = \frac{d^2 v_2(t)}{dt^2}$$

$$\dot{X}2 = \frac{dv_2}{dt}$$

$$\dot{\mathbf{X}} = \begin{bmatrix} 0 & 1 \\ \frac{-1}{\mathrm{LC}} & \frac{-\mathrm{R}}{\mathrm{L}} \end{bmatrix} \mathbf{X} + \begin{bmatrix} 0 \\ \frac{1}{\mathrm{LC}} \end{bmatrix} V_1 \tag{1.6}$$

$$\mathbf{Y} = \begin{bmatrix} 1 & 0 \end{bmatrix} \mathbf{X} + [0]v_1 \tag{1.7}$$

Where,

$$\mathbf{X} = \begin{bmatrix} v_2 \\ \frac{dv_2}{dt} \end{bmatrix}$$

and

$$\dot{\mathbf{X}} = \begin{bmatrix} \frac{dv_2}{dt} \\ \frac{d^2 v_2(t)}{dt^2} \end{bmatrix}$$

Transfer Function Models

In control systems another common way of defining a system is by its transfer function in frequency domain where the input and output equations are differential equations in s. One way to measure the performance of a system and determine its stability is to look at the solutions of these differential equations which are called poles and zeros.

For example the continuous form of the lumped system shown in block diagram of Figure 1.5 in s-domain can be represented as in Figure 1.7. With $\mathbf{U}$(s) and $\mathbf{Y}$(s) as the Laplace transforms of the inputs $\mathbf{u}$(t) and output $\mathbf{y}$(t) the transfer function of the system can be given by 1.8,

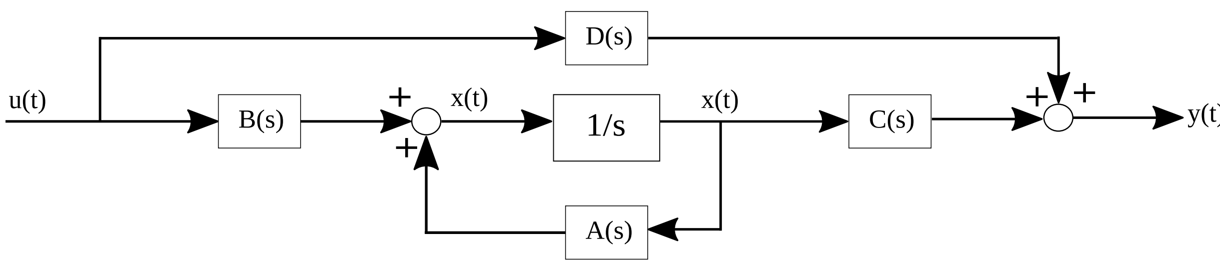

Fig. 1.7.: Block Diagram of a continuous system in s-domain.

$$\begin{aligned} \mathbf{H}(s) &= \frac{\mathbf{Y}(s)}{\mathbf{U}(s)} \\ &= \mathbf{B}(s)\left(\frac{1}{s-\mathbf{A}(s)}\right)\mathbf{C}(s)+\mathbf{D}(s) \end{aligned} \tag{1.8}$$

For the RLC series circuit in Figure 1.6 the transfer function model is given by Equation 1.9. Applying KVL in the circuit we get,

$$\begin{aligned} v_1 - CR\frac{dv_2}{dt} - LC\frac{d^2v_2}{dt^2} - v_2 = 0 \\ V_1(s) - CRsV_2(s) - LCs^2V_2(s) - V_2(s) = 0 \\ \frac{V_2(s)}{V_1(s)} = \frac{1}{1+sRC+s^2LC} \end{aligned} \tag{1.9}$$

The roots of the characteristics equations in the numerator and denominator of the transfer function are the zero and poles respectively. The transfer function model however, maps the input-output relation only without giving any insight into its inner state variables.

1.2.3 Kalman Filter Model

Kalman filter is a Least-Square Estimation algorithm, that operates in time domain and in a recursive manner. It refines its estimation by minimizing the covariance between the true signal and its estimation and does so by updating its old estimation for every new measurement in time. These two concepts will be better understood as we proceed through this section and explain the algorithm.

With a system defined in a state space model as in Equation 1.1 and Equation 1.2, the Kalman filter is used to estimate $\mathbf{X}$, the state variable at each point in time, which in turn is used to calculate the output estimate $\mathbf{Y}$. The relationship between the observations or measurements, $\mathbf{Z}$ made with the process and state variable $\mathbf{X}$ can be modeled with the linear relation Equation 1.10

$$\mathbf{z}_k = \mathbf{H}_k\mathbf{x}_k + \mathbf{D}_k\mathbf{u}_k \tag{1.10}$$

Here,

$\mathbf{z}_k$ = the observed value of the process at time t_k.

$\mathbf{H}_k$ = Measurement sensitivity matrix, that transforms the state space variable parameters into the measurement domain. For example if we were to estimate velocity, that is, the state variables are velocities at each point in time and the observations made was distances then $\mathbf{H}$ would be Δt. An important assumption in Kalman algorithm is that all the parameters and state variables used to define the system are Gaussian in nature and as a result the estimates calculated are Gaussian in nature.

Both the system definition and the measurement process come with a certain level of uncertainty. This uncertainty can be incorporated in the system model as well as measurement model by modifying Equation 1.1 and 1.10 as

$$\mathbf{x}_{k+1} = \mathbf{A}_k\mathbf{x}_k + \mathbf{B}_k\mathbf{u}_k + \mathbf{w}_k \tag{1.11}$$

$$\mathbf{z}_k = \mathbf{H}_k\mathbf{x}_k + \mathbf{D}_k\mathbf{u}_k + \mathbf{v}_k \tag{1.12}$$

$\mathbf{w}$ and $\mathbf{v}$ are process error and measurement error respectively and are both modeled as white noise and thus are uncorrelated. The covariance matrices for these parameters are respectively $\mathbf{Q}$ and $\mathbf{R}$ given by Equation 1.13 and Equation 1.14,

$$E[\mathbf{w}_k \mathbf{w}_i] = \begin{cases} \mathbf{Q}_k & i = k \\ 0 & i \neq k \end{cases} \tag{1.13}$$

$$E[\mathbf{v}_k \mathbf{v}_i] = \begin{cases} \mathbf{R}_k & i = k \\ 0 & i \neq k \end{cases} \tag{1.14}$$

Thus, $\mathbf{Q}$ and $\mathbf{R}$ are the parameters that quantify the uncertainty associated with system model and measurement process respectively.

The entire algorithm can be divided into two stages, predictor stage or Time Update stage [12] where a prior prediction is made and the time point is updated and corrector stage or Measurement Update stage where this initial estimate made in the predictor stage is updated.

At first, in the predictor stage, the estimate, $\hat{\mathbf{x}}_{k-1}$ from the previous time point is taken to make an *apriori* estimate of the state of the system at present time point, $\hat{\mathbf{x}}_k^-$ based on the system definitions and the reference input $\mathbf{U}$ with Equation 1.15. At the start however when there is no previous time point data a blind initial estimate is made prior to any knowledge of the system to be used to predict the state of the system at that point in time.

$$\hat{\mathbf{x}}_k^- = \mathbf{A}_k \hat{\mathbf{x}}_{k-1} + \mathbf{B}_k \mathbf{u}_k \tag{1.15}$$

The *apriori* estimation error is defined as,

$$\mathbf{e}_k^- = \hat{\mathbf{x}}_k^- - \mathbf{x}_k \tag{1.16}$$

And the parameter that quantifies the uncertainty in the estimation process is the estimation error covariance matrix, $\mathbf{P}$. Thus the *apriori* estimation covariance is given by,

$$\mathbf{P}_k^- = E[\mathbf{e}_k^- \mathbf{e}_k^{-T}] \tag{1.17}$$

From Equations 1.15, 1.16 and 1.17, the *apriori* estimation covariance matrix equation for the current time point is obtained,

$$\mathbf{P}_k^- = \mathbf{A}_k \mathbf{P}_{k-1} \mathbf{A}_k^T + \mathbf{Q}_k \tag{1.18}$$

In the corrector stage, these current time point *apriori* estimations, $\hat{\mathbf{x}}_k^-$ and $\mathbf{P}_k^-$ are taken and based on the current process measurement $\mathbf{z}_k$, input $\mathbf{u}_k$, and Kalman gain $\mathbf{K}$ updated state estimation $\mathbf{x}_k$ and the updated estimation covariance $\mathbf{P}_k$ is determined.

The updated estimation is a linear combination of the *apriori* estimation, $\hat{\mathbf{x}}_k^-$ and a weighted difference between the measurement, $\mathbf{z}_k$, and measurement prediction,$(\mathbf{H}_k\hat{\mathbf{x}}_k^- - \mathbf{D}_k\hat{\mathbf{u}}_k)$, as shown in Equation 1.20. This difference is called measurement innovation, showing the discrepancy between the predicted measurement and actual measurement [12] . The weighting factor, Kalman gain $\mathbf{K}$, updates the estimation based on the estimation covariance matrix, $\mathbf{P}$ and measurement noise covariance matrix $\mathbf{R}$. When the observations are less noisy thus more accurate but there is not much known about the system itself making the system model as well as estimation possess comparatively highly uncertain, $\mathbf{K}$ favors the measured values more than the *apriori* estimates. The opposite is also true, When the system measurement process is noisy, and the system definition is comparatively accurate $\mathbf{K}$ favors the initial estimates over the measurements to obtain the updated estimate for each time point. The expression for $\mathbf{K}$ is given as,

$$\mathbf{K}_k = (\mathbf{P}_k^- \mathbf{H}_k^T)/(\mathbf{H}_k \mathbf{P}_k^- \mathbf{H}_k^T + \mathbf{R}_k) \tag{1.19}$$

And the state estimation as well as estimation covariance update is given by,

$$\hat{\mathbf{x}}_k = \hat{\mathbf{x}}_k^- + \mathbf{K}_k(\hat{\mathbf{z}}_k - \mathbf{H}_k\hat{\mathbf{x}}_k^- - \mathbf{D}_k\hat{\mathbf{u}}_k) \tag{1.20}$$

$$\mathbf{P}_k = (\mathbf{I} - \mathbf{K}_k\mathbf{H}_k)\mathbf{P}_k^- \tag{1.21}$$

The output estimate $\hat{\mathbf{y}}_k$ is calculated from the estimated state variable $\mathbf{x}_k$

$$\hat{\mathbf{y}}_k = \mathbf{C}_k\hat{\mathbf{x}}_k + \mathbf{D}_k\mathbf{u}_k \tag{1.22}$$

$\hat{\mathbf{x}}_k$ and $\mathbf{P}_k$ are used as the *apriori* state estimate and estimation covariance respectively for the next time point estimation. This way each time point estimation retains all the previous time point estimations and makes the algorithm recursive. The block diagram of Figure 1.8 adopted from 'An Introduction to the Kalman Filter' [12] summarizes the process

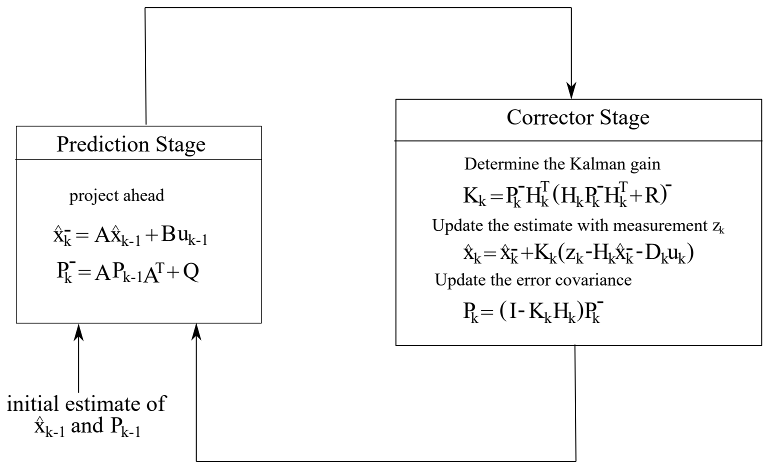

Fig. 1.8.: Kalman filter estimation Block Diagram.

1.2.4 System Characterization: Transfer Function Estimation

Kalman Filter and its various modifications is being used for estimating system parameters, tracking state of systems and denoising signals for years. Here we use its denoising by signal estimation scheme for system characterization.

The way the use-case characterization is realized is a well-known input, a reference signal, is fed into the UIA using a second channel. UIA mixes this signal with the captured signals of interest and a mixed response is recorded as its output. However since the reference input $\mathbf{R}$ is known, its response $\mathbf{Y}$ can be estimated from within the mixed signal response using Kalman filter as shown in Figure 1.9 .

Then the estimated transfer function for this particular recorded signal becomes,

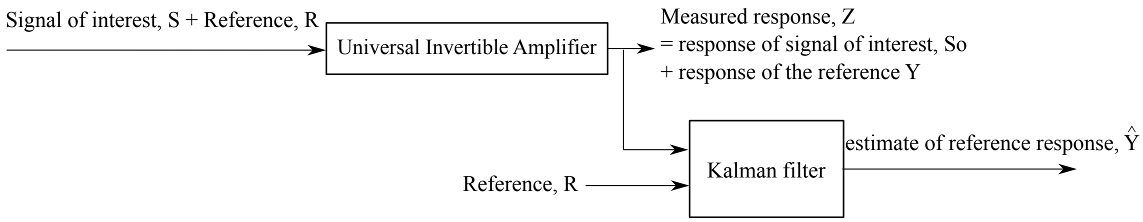

Fig. 1.9.: Transfer function estimation Block Diagram.

$$\mathbf{TF} = \frac{\hat{\mathbf{Y}}}{\mathbf{R}} \tag{1.23}$$

Two different approaches were taken for feeding a reference to the system,

- Using a digitally synthesized noise signal to capture the signal characteristics across a wide band of frequencies. In this case the synthesized reference needs to be fed through the second channel of UIA, Figure 1.10.

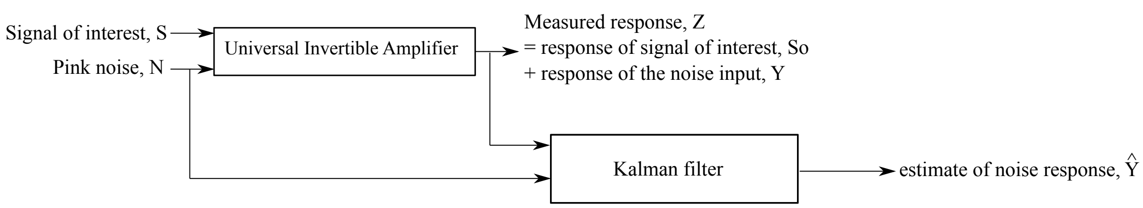

Fig. 1.10.: Transfer function estimation using external noise reference.

- Using an inherent bio-signal with well known characteristics. This cancels the requirement of a second input channel in UIA but requires a second recording channel to capture the well characterized bio-signal as seen at the input of the UIA in order to provide Kalman filter with a reference input to track its response. In our case the well known signal is Electrocardiogram, ECG which in most cases is contaminated with the signal of interest, Figure 1.11.

For both cases Kalman filter considers the signal of interest as noise and the injected noise, which is the reference, as signal of interest, filtering out everything but the reference response, which in turn is used to generate a transfer function estimate.

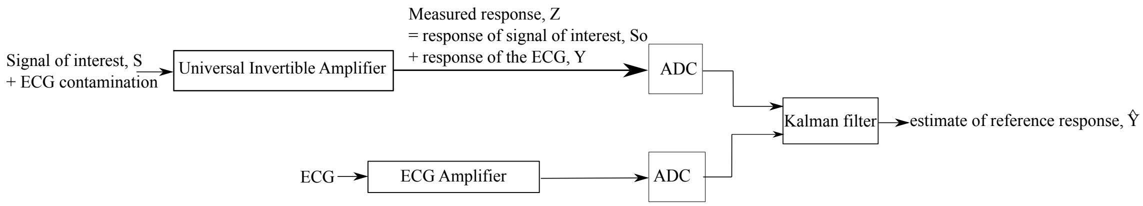

Fig. 1.11.: Transfer function estimation using inherent bio-signal reference.

A problem that was faced with estimating a second order transfer function was that the estimation tended to go out of bound and would produce unstable results. Splitting the transfer function into two first order transfer functions solved the problem. This way two separate measurements were recorded from the two stages of UIA and they were used to estimate the two different transfer functions, combining them in the end to produce the final transfer function.

1.3 Objectives

The aims of this thesis was:

- Implementation and characterization of a higher order Universal Invertible Amplifier, and
- Implementation of a use-case characterization schema.

These aims and their implementation is discussed in the later chapters.

2. UNIVERSAL INVERTIBLE AMPLIFIER: SECOND GENERATION

The first generation of Universal Invertible Amplifier was a low noise variable gain architecture that comprised the entire bio-signal spectrum with a profile complementing the bio-signal spectrum. This was using OEIE algorithm as a means to characterize the system [1]. However a need for higher gain, lower noise variable gain system with more robust characterization scheme was evident, which prompted the design of second generation UIA.

One of the main focus for UIA was detection of very low amplitude nerve signal which could be on the order of 10 μ V. The total noise of the system, which included thermal noise produced by the different the components in the system was contributing an input to output referred noise [13] equivalent of 30 μV which essentially buries the signal of interest. This necessitated the design of a quieter system. For similar reasons A higher gain at 1 Khz - 10 Khz frequency, where these nerve signals lie was necessary. These modifications in the UIA architecture will be discussed in the following sections in this chapter.

The Output Error Input Error algorithm used to characterize the first generation UIA is a transfer function estimation algorithm, that is applicable for benchtop characterization before or after the use of the system. The second generation UIA being fourth order system (Second order compressor and second order expander) is more susceptible to instability and transfer function shift thus requires a characterization scheme that is real-time. Kalman filter algorithm is used to estimate the response of a known reference input instead of directly estimating the transfer function and the estimated response and reference is used to determine the system characteristics. The system characterization scheme will be discussed in later chapters.

2.1 UIA Architectures

The universal aspect of the UIA comes from the fact that its gain bandwidth property encompasses the entire bio-signal spectrum making it universally applicable to all common bio-signals. The same gain bandwidth property that has a defined gain at all the frequencies of interest down to DC signal makes it invertible. No signal is permanently distorted by the amplifier-filtering architecture of the UIA. These are the common properties maintained throughout all the iterations of its modification.

The first generation UIA, UIA01 is described in Chapter 1, the modifications in the architecture and improvements in the characteristics of the second generation UIA, UIA02 and UIA03, are presented in this chapter.

2.1.1 Second Order UIA: UIA02 and UIA03

The need for the design of a second generation of UIA, a second order amplifier-filter system, was the requirement of a higher gain profile at high frequency region for the low amplitude nerve signal recording. Two different prototypes were developed as second generation UIA, UIA02 and UIA03.

UIA02

UIA02, Figure 2.1, consists of two INA 111 at its front end giving it an additional channel for injecting reference. This headstage provides for a flat gain of 2 at all frequencies. The second stage is another INA 111 with a variable gain profile of 1-50 over frequencies DC-40 KHz. The second order variable gain of 1-100 over the same spectrum was introduced by precession amplifier OPA228. The total gain bandwidth profile, 2-10000 over DC-40 KHz, of UIA02 is shown in Figure 2.2. Its benchtop characterization shows stability up to 40 KHz. The component values incorporated in the circuit of Figure 2.1 to produce the frequency response of Figure 2.2 are R1 and R2 equal to 50KΩ, R3 and R4 equal to 1KΩ and R5 equal to 100 KΩ. UIA02 transfer function is,

$$TF_{02} = \frac{10004(s + 19.6)(s + 10)}{(s + 1000)(s + 980.4)} \tag{2.1}$$

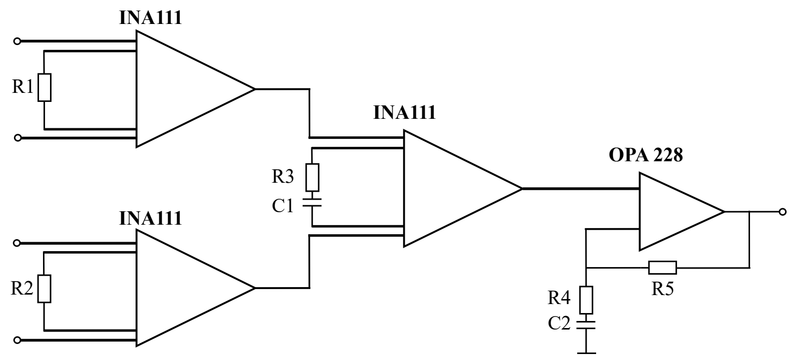

Fig. 2.1.: UIA02 circuit diagram.

Even though UIA02 fulfilled the requirement of a stable higher gain second order system, the additional INA 111s were adding to the noise. The input referred noise [13] caused by the higher feedback resistances in its internal circuit was increasing the noise level above our signal of interest, the neural activity. Thus a low noise system design was developed with UIA03.

UIA03

In UIA03 architecture, Figure 2.3, the INA 111 was replaced with low noise instrumentation amplifier, INA 217 [14]. The high impedance headstage was removed and a separate unity gain high impedance preamplifier was used to communicate with the electrodes along with a spatial averaging circuit added to the preamplifier, making the UIA architecture smaller.

The gain profile of UIA03 was reduced to 1-5000, Figure 2.4, from gain of 2-10000 in UIA02 by the removal of INA 111 headstage. The variable gains in the first stage (1-100 over its bandwidth) and second stage (1-50 over its bandwidth) were also

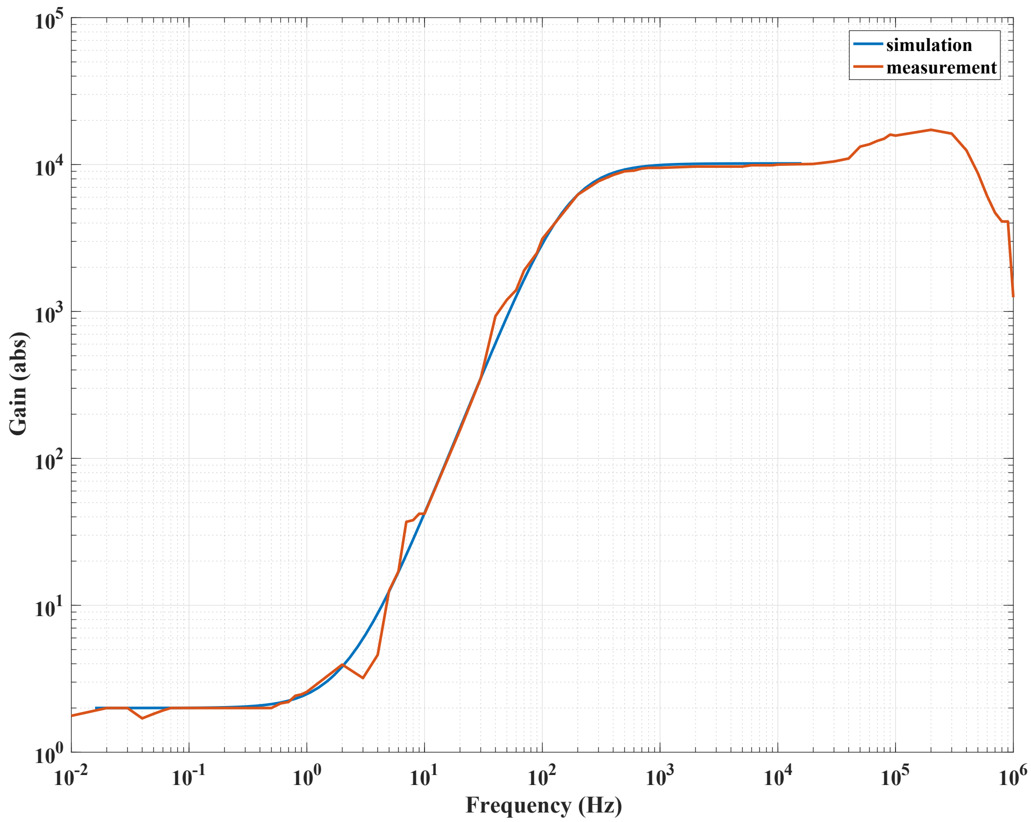

Fig. 2.2.: UIA02 frequency response.

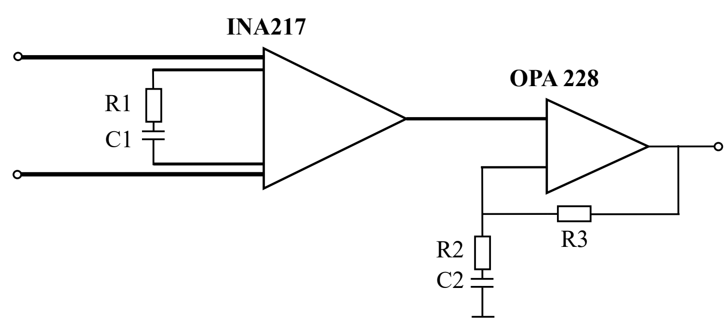

Fig. 2.3.: UIA03 circuit diagram.

switched. The reason was to reduce the resistor values required in the circuit reducing overall thermal noise. The component values implementing these changes for the circuit in Figure 2.3 are R1 = 100Ω, C1 = 10μF, R2 = 50Ω, R3 = 2.5KΩ and C2 = 47μF.

The transfer function for UIA03 is,

$$TF_{03} = \frac{5151(s + 9.901)(s + 8.344)}{(s + 1000)(s + 425.5)} \tag{2.2}$$

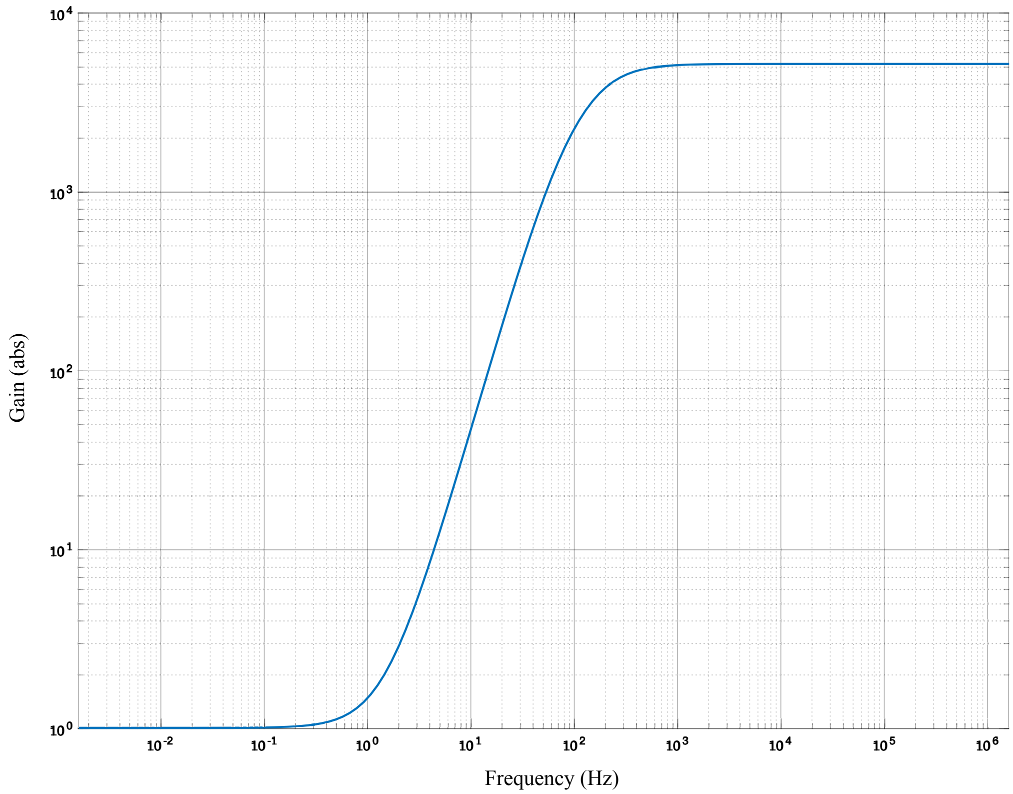

Fig. 2.4.: UIA03 frequency response.

UIA03 was the final second order UIA architecture used for data recording and evaluation of transfer function estimation process.

2.2 Use Cases: Signal Extraction

For validation of the Universal and invertible architecture, UIA03 was used for ECG and EMG extraction. ECG Data was collected from rat vagus nerve while EMG data was collected from human muscle.

2.2.1 ECG Extraction

Vagus nerve data from Sprague Dawley rats was used for ECG extraction. All the procedures were carried out according to protocol SC235R approved by IUPUI School of Science Animal Resource Center (SARC) Institutional Animal Care and Use Committee (IACUC). The vagus nerve was accessed through a chest opening in an anesthetized rat using Transverse Intrafascicular Multichannel Electrodes, TIMEs. Adequate anesthesia was maintained during the entire procedure. At the end of the procedure the rat was euthenized according to protocol.

For recording the amplified data from UIA an ADAT recording system along with Cubase VST32 software was used. A standard flat amplifier was also used for simultaneous amplification and recording to validate the extracted data using UIA.

The recorded output, Figure 2.5 after inversion was reduced to the data seen by the electrode. ECG extraction was done by bandpass filtering the inverted data within the bandwidth, 0.2Hz-200Hz [3]. It shows close match with the ECG signal collected using the standard amplifier, Figure 2.6. The difference in amplitude can be attributed to the difference in signal sources, since the standard amplifier data was collected from across the chest using hypodermic needle electrode whereas the UIA data was collected from Vagus nerve using TIMEs. But the phase match for P-wave an the QRS-complex is considered successful extraction in this case.

2.2.2 EMG Extraction

EMG data was collected from human muscle using Ag/AgCl surface electrode (MEDITRACE 530 series, gel type adhesive). Prior to data collection the skin was prepped by abrasion using medical grade sand paper for skin impedance reduction.

For recording the amplified data NIDAQ (NI USB 6212) and Mr. Kick version III was used. EMG data was extracted using bandpass filter within the bandwidth, 200Hz-2KHz [3]. The extracted EMG showed close match with the EMG data

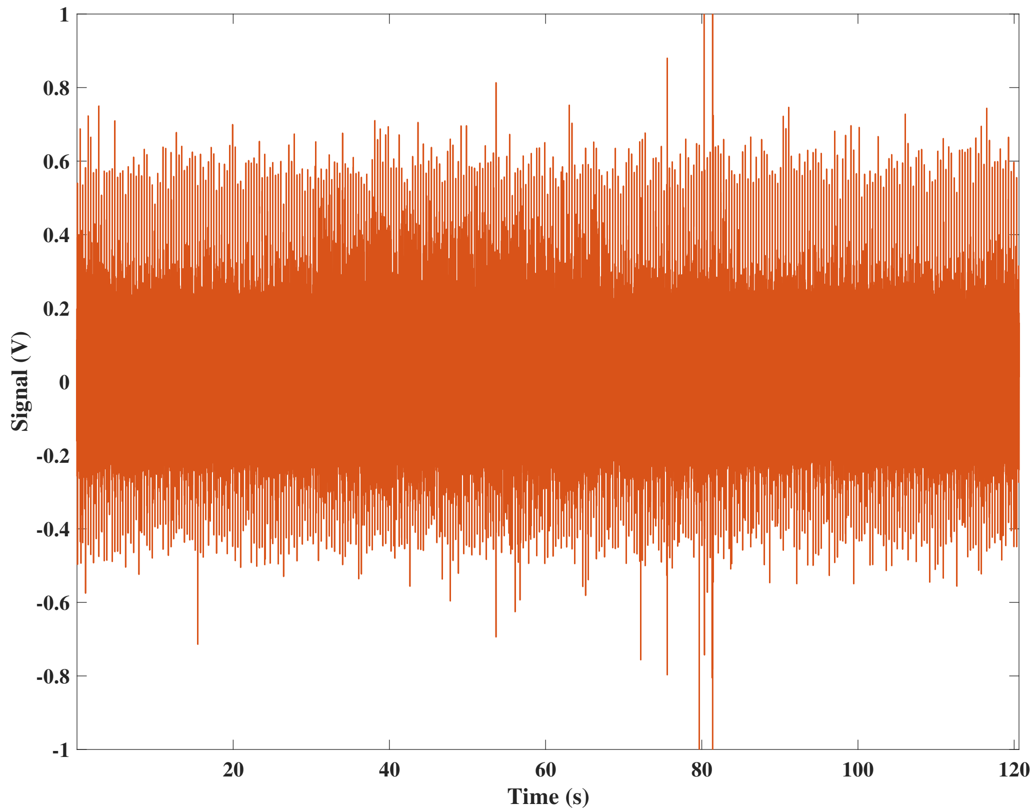

Fig. 2.5.: Mixed and compressed signal at the output of UIA.

recorded with the standard amplifier Figure 2.8 Figure 2.9. The mean error between the extracted EMG from UIA and the standard amplifier was 0.02 μV.

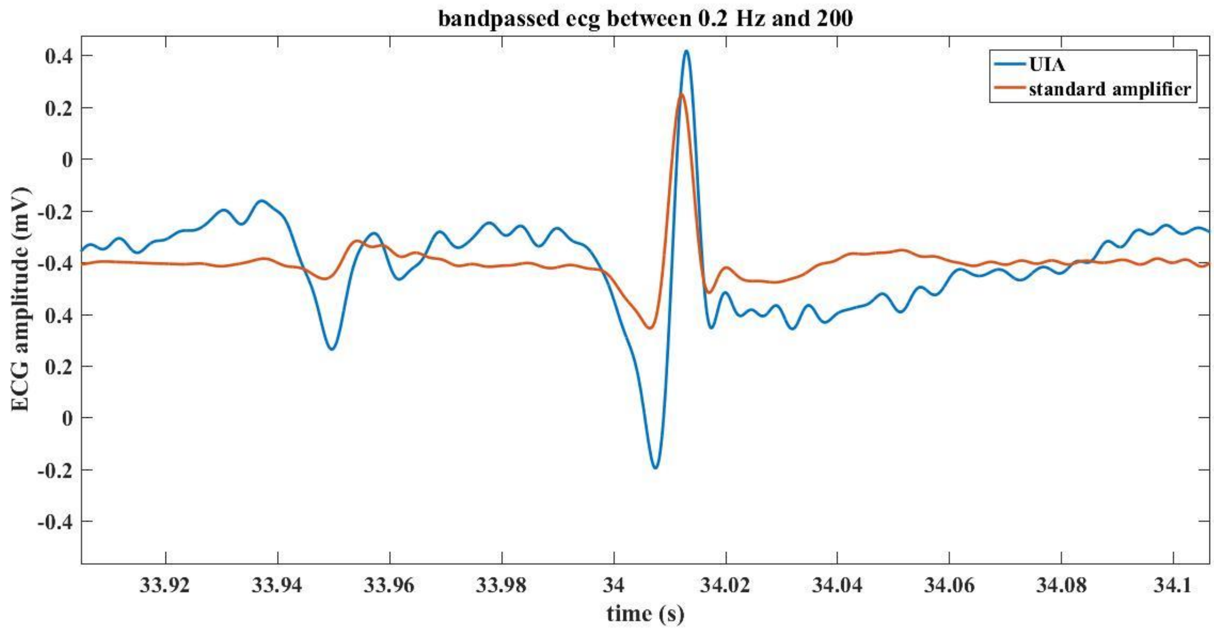

Fig. 2.6.: ECG extracted from the UIA output by bandpass filtering the inverted signal between 0.2Hz and 200Hz.

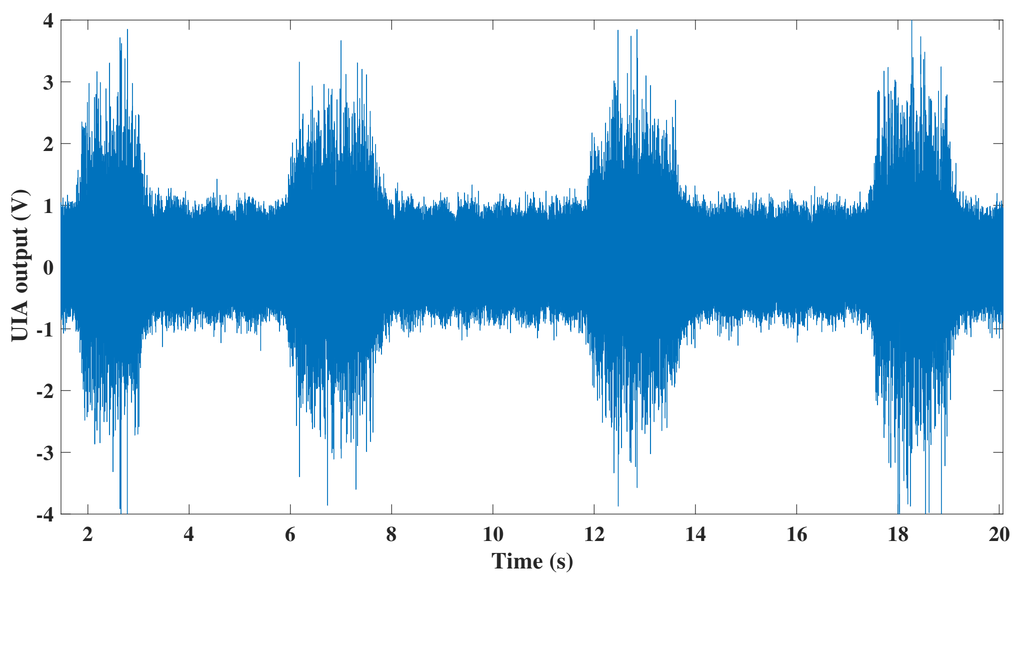

Fig. 2.7.: Mixed signal at the output of UIA.

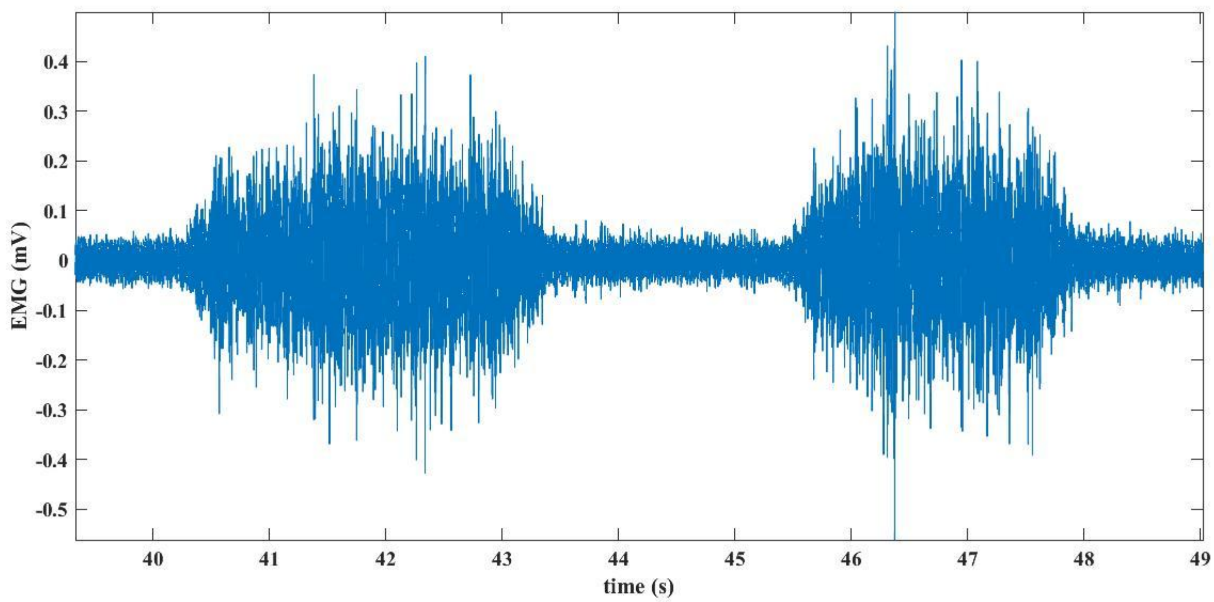

Fig. 2.8.: Extracted EMG from inverted UIA output using bandpass filer between 200Hz and 2KHz. the signal show muscle contraction and relaxation.

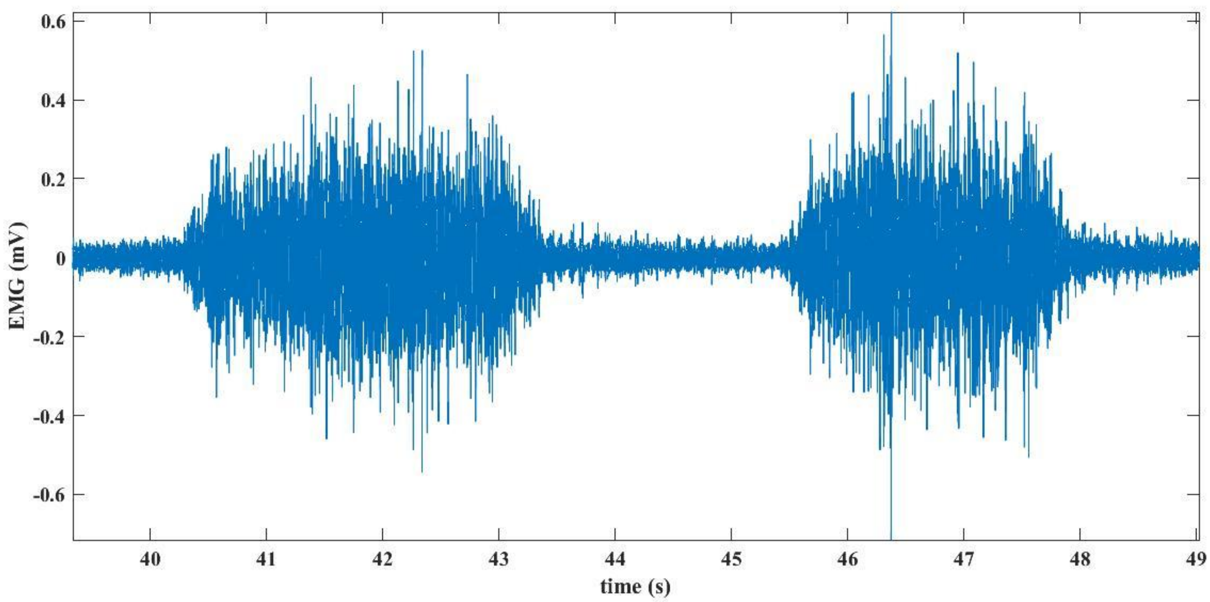

Fig. 2.9.: Simultaneous EMG recorded using a standard amplifier showing the same muscle contraction and relaxation matching UIA data extraction.

3. A CASE FOR CONTINUOUS CHARACTERIATION AND INTRODUCTION TO TRANSFER FUNCTION ESTIMATION

Most systems have a range of variance in its performance depending on the environment conditions such as temperature or usage condition such as source power etc., which is normally mentioned in their user manual. This holds true for Universal Invertible Amplifier, UIA too. Each of the component used in its design have their own variance factors which can multiply to produce a transfer function drift substantial enough that will throw off the inversion process.

Several error analyses were run simulating conditions where different components were introduced with different percentage errors in their values and the UIA inversion performance against the calculated total shifted transfer function was evaluated and was found to be substantial for small scale signals. This validated the necessity to know the actual transfer at the time of amplifying. All the simulations were run in Matlab 2016b.

The first attempt at use-case characterization was to use a known reference signal, digitally generated noise, as a second input to the UIA and estimating its output using Kalman filter. The estimation performance was perfect at higher frequency region but was not that great at lower frequency region.

3.1 Inversion Error Analysis

The inversion error analyses were done in simulation to reflect various shifts in three different component values in UIA architecture that can happen over time, change of temperature or usage condition. Resultant transfer function shift for shifts in different component was calculated by the method of propagation of error [15] .

For inversion simulation, software generated White Gaussian Noise was used with micro level amplitude.

3.1.1 Transfer Function Shift Calculation

Two capacitor values and one resistor values were varied in random within a range of ±50% of their values. These components were chosen because they formed the poles as the shift in poles contributes largely to the instability. The resulting transfer function was calculated using equation of error propagation [15] as.

$$\frac{dH}{H} = \frac{dR}{R} + \frac{dC1}{C1} + \frac{dC2}{C2} \tag{3.1}$$

$$\textit{percentage of transfer function error} = \frac{dH}{H} \times 100\% \tag{3.2}$$

Where dH, dR, dC1, and dC2 are the changes in the values of the transfer function, H, resistor, R, capacitor, C1 and second capacitor C2.

For each shift, dH, mean of the inversion error was calculated.

3.1.2 Inversion Error calculation for Varying Shifts in Transfer Function

10000 random cases of dH shifts corresponding to 10000 random combination of the three component shift were taken for inversion error simulation for a known noise input, *N(t)*. The block diagram of Figure 3.1 shows the procedure.

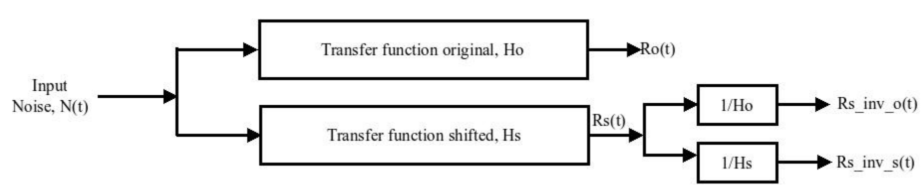

Fig. 3.1.: Block diagram for error analysis.

The response, *Rs(t)* of *N(t)* to the shifted transfer function, Hs was inverted using both the original transfer function, Ho giving Rs_inv_o(t) and the shifted transfer function, Hs giving Rs_inv_s. For the inversion to be accurate the inverted signal should match *N(t)*. Inverting with Hs compensates for the shift in transfer function during recording the response and thus the inverted signal, Rs_inv_s should show no difference from the *N(t)*. However, it shows a significantly small amount of difference which can be accounted as computational errors. The inverted signal Rs_inv_o which was not compensated for transfer function shift in comparison shows considerable difference. Median value was taken as a measure of the average error for each transfer function shift.

Figure 3.2 shows the error level in inversion without shift compensation for varying shifts in transfer function. Here the transfer function errors are sorted and grouped within interval of 5% of error and mean of the inversion error within every interval is plotted along with the upper quartile and lower quartile values within that interval.

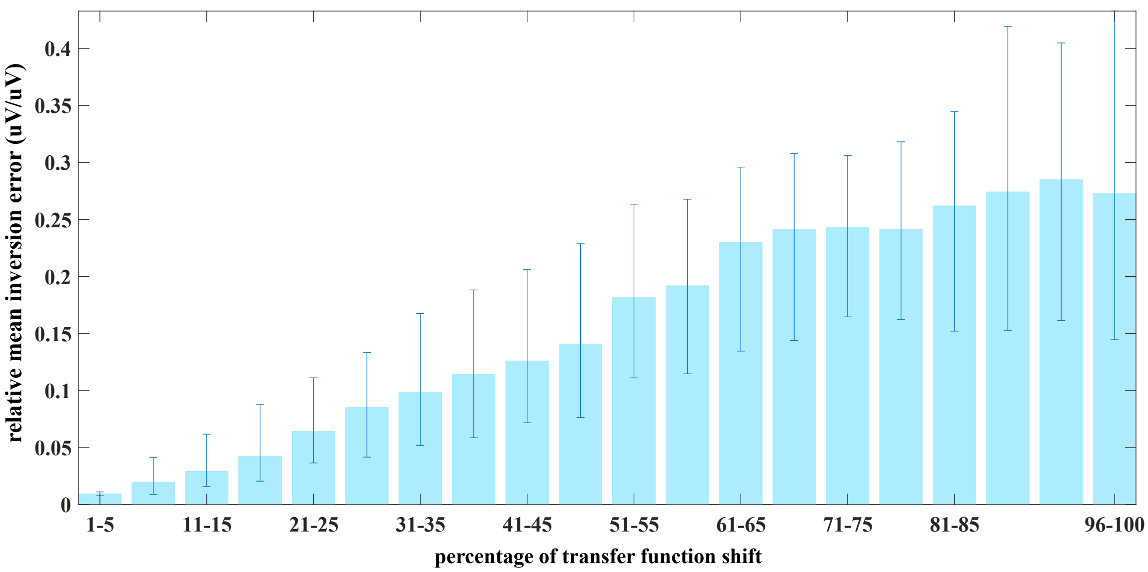

Fig. 3.2.: Inversion error in shift uncompensated inversion.

Figure 3.3 shows the inversion error with transfer function shift compensation. A similar approach of plotting the mean inversion error within an interval of 5% transfer function shifts was taken. From a comparison of Figures 3.2 and 3.3 with the same transfer function shift of 15%-20%, which corresponds to a variance of around 5%-6.67% for each of the components, the mean inversion error becomes 4% whereas in the case of shift compensated inversion, error lies at 0.3%. The inversion error in case of shift compensation does not depend too much on the transfer function shifts and has an almost constant level of around 0.3% within the entire range of error calculation. This error can be attributed to computational errors and can be considered insignificant.

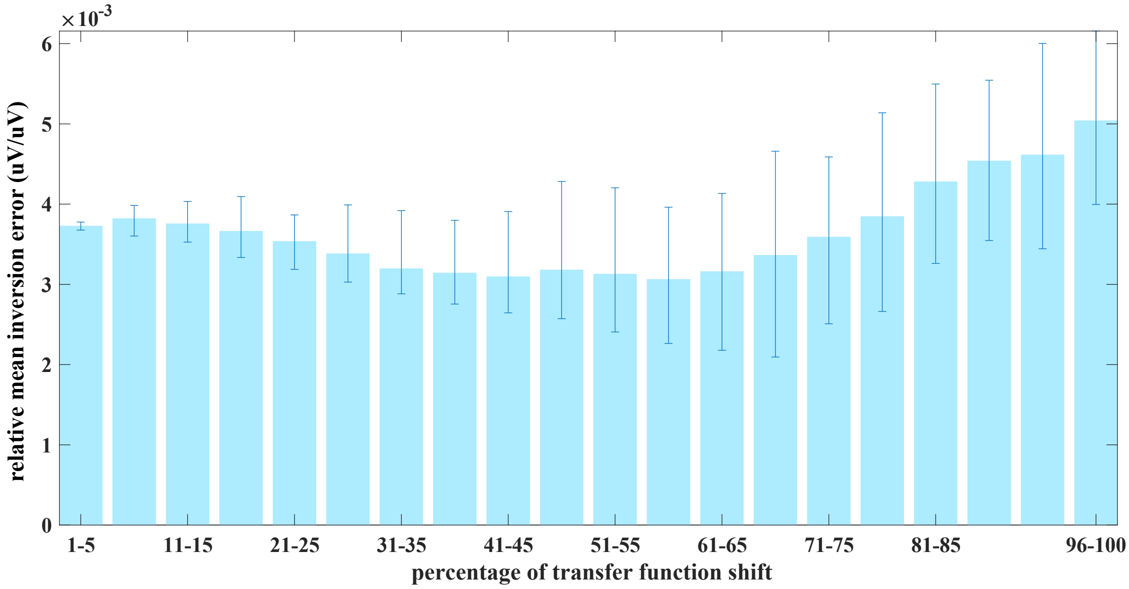

Fig. 3.3.: Inversion error in shift compensated inversion.

3.2 Transfer Function Estimation Process

The process for transfer function estimation was briefly introduced in Chapter 1. To find out the transfer function of the system either the component values of the system need to be measured or it can be estimated from a known input-output pair. Measuring the component values is not possible while the system is being used. So we use a known input-output pair to estimate the transfer function or system characteristics.

However, even if we consider a perfect error less recording setup, only the recorded output is known and the input is unknown. If an additive known input is introduced into the system along with the signal of interest, its response will be mixed with the response of the signal of interest to the system. Thus at that point the output of the known input is unknown.

Thus we use the Kalman filter estimation algorithm introduced in Chapter 1 to track the response of the known input to the system, filtering out other responses and estimate the transfer function using the known input-estimated output pair with Equation 1.23, as shown in Figure 3.4.

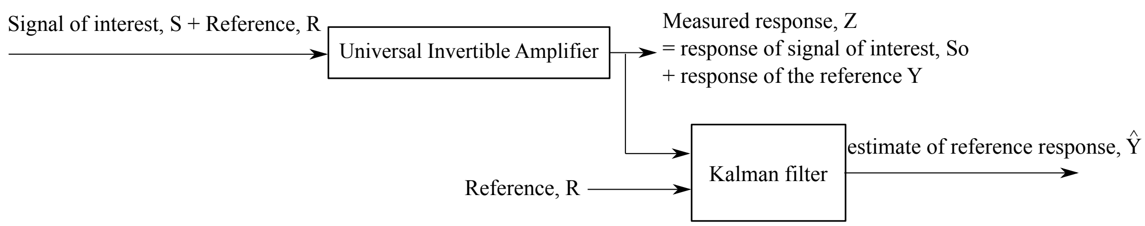

Fig. 3.4.: Transfer function estimation Block Diagram.

The two cases evaluated for estimating the response of a known input are,

1. Using a digitally synthesized input. This use-case and its outcomes are discussed in details in the following section, Section 3.3

2. Using a well-defined bio-signal that is naturally collected by the recording system along with the signal of interest, i.e. a well-defined inherent noise, which is discussed in Chapter 4.

The Kalman filter estimation process that is used to track the response of the known reference signal in the mixed output is described in Chapter 1. For ease of explanation the equations will be presented in brief in this Chapter too.

After the development of the algorithm, it was tested for known input-output pair in simulation for characterizing its estimation performance.

3.2.1 Kalman Filter Estimation

For Kalman filter estimation the UIA system needs to be defined in state space model. The UIA in transfer function model is given by,

$$TF = \frac{5151(s + 9.901)(s + 8.344)}{(s + 1000)(s + 425.5)} \tag{3.3}$$

In state space model the discrete form of UIA transfer function is

$$\mathbf{X}_k = \begin{bmatrix} 1.863 & -0.8671 \\ 1 & 0 \end{bmatrix} \mathbf{X}_{k-1} + \begin{bmatrix} 32 \\ 0 \end{bmatrix} \mathbf{U}_{k-1} \tag{3.4}$$

$$\mathbf{Y}_k = \begin{bmatrix} -21.43 & 20.79 \end{bmatrix} \mathbf{X}_k + 5151\mathbf{U}_k \tag{3.5}$$

With,

$$\mathbf{A} = \begin{bmatrix} 1.863 & -0.8671 \\ 1 & 0 \end{bmatrix} \tag{3.6}$$

$$\mathbf{B} = \begin{bmatrix} 32 \\ 0 \end{bmatrix} \tag{3.7}$$

$$\mathbf{C} = \begin{bmatrix} -21.43 & 20.79 \end{bmatrix} \tag{3.8}$$

$$\mathbf{D} = 5151 \tag{3.9}$$

Equation 3.4 and Equation 3.5 becomes,

$$\mathbf{X}_k = \mathbf{A}\mathbf{X}_{k-1} + \mathbf{B}\mathbf{U}_{k-1} \tag{3.10}$$

$$\mathbf{Y}_k = \mathbf{C}\mathbf{X}_k + \mathbf{D}\mathbf{U}_k \tag{3.11}$$

Here, $\mathbf{A}$, $\mathbf{B}$, $\mathbf{C}$ and $\mathbf{D}$ represents the State transition matrix, Input Coupling matrix, Output coupling matrix and Feed through matrix respectively of the system. The UIA being time-invariant $\mathbf{A}$, $\mathbf{B}$, $\mathbf{C}$ and $\mathbf{D}$ are all constant in this case.

And from Equation 1.10 the known reference input in this case is $\mathbf{U}$ and its response is $\mathbf{Y}$. The measurement equation is as given by Equation 3.12

$$\mathbf{Z}_k = \mathbf{H}\mathbf{X}_k + \mathbf{D}\mathbf{U}_k \tag{3.12}$$

With,

$$\mathbf{H} \quad = \quad \begin{bmatrix} -21.43 & 20.79 \end{bmatrix} \tag{3.13}$$

$$\tag{3.14}$$

In this case measurement sensitivity matrix $\mathbf{H}$ is the same as $\mathbf{C}$ since the estimated output $\mathbf{Y}$ and the measured signal $\mathbf{Z}$ have the same units of measurement, V. $\mathbf{Z}$ in this case is the mixed response $\mathbf{Y}+\mathbf{So}$, Figure 3.4. It treats $\mathbf{S}$ as noise and estimates $\mathbf{Y}$, essentially filtering out the noise $\mathbf{So}$.

In the prediction stage an *apriori* estimate of the state variable $\mathbf{X}$ and estimation covariance $\mathbf{P}$ is made with Equations 3.15 and 3.16. At time point zero where no previous time point estimate is not available the initial estimate $\hat{\mathbf{x}}_{k-1}$ was set to be equal to zero, and since this was a blind estimate which potentially is very far from the actual measurement, the initial $\mathbf{P}_{k-1}$ was set a relatively high value. Once the estimate stabilizes the covariance at steady state becomes small too.

$$\hat{\mathbf{x}}_k^- = A\hat{\mathbf{x}}_{k-1} + B\mathbf{u}_k \tag{3.15}$$

$$\mathbf{P}_k^- = \mathbf{A}_k\mathbf{P}_{k-1}\mathbf{A}_k^T + \mathbf{Q}_k \tag{3.16}$$

In the corrector stage the *apriori* estimate of state variable and its covariance are updated using Kalman gain $\mathbf{K}$ and the measured signal $\mathbf{Z}$ by Equations 3.18 and 3.19

$$\mathbf{K}_k = (\mathbf{P}_k^-\mathbf{H}_k^T)/(\mathbf{H}_k\mathbf{P}_k^-\mathbf{H}_k^T + \mathbf{R}_k) \tag{3.17}$$

$$\hat{\mathbf{x}}_k = \hat{\mathbf{x}}_k^- + \mathbf{K}_k\mathbf{z}_k - \mathbf{H}_k\hat{\mathbf{x}}_k - \mathbf{D}_k\hat{\mathbf{u}}_k) \tag{3.18}$$

$$\mathbf{P}_k = (\mathbf{I} - \mathbf{K}_k\mathbf{H}_k)\mathbf{P}_k^- \tag{3.19}$$

The estimate updates depend on Kalman gain $\mathbf{K}$ which in turn depends on process noise, $\mathbf{Q}$, and measurement noise, $\mathbf{R}$ [16]. Thus one way to manipulate the estimation process is to manipulate these two parameters. In our case we were confident with the system definition to keep $\mathbf{Q}$ small but with the actual signal of interest being the noise to be filtered in the estimation algorithm $\mathbf{R}$ was set to be relatively large.

The response estimate, $\hat{\mathbf{Y}}$ to the known reference $\mathbf{U}$ can be calculated by 3.20

$$\hat{\mathbf{Y}}_k = \mathbf{C}\hat{\mathbf{X}}_k + \mathbf{D}\mathbf{U}_k \tag{3.20}$$

The estimation algorithm was developed as a Matlab code and all estimation processing including estimation error evaluation was done in Matlab 2016b.

3.2.2 Kalman Filter Estimation Performance

To test the performance of the code for estimation developed in Matlab, A software generated square-wave input and its response to the UIA transfer function was used. A block diagram of the process is shown in Figure 3.5.

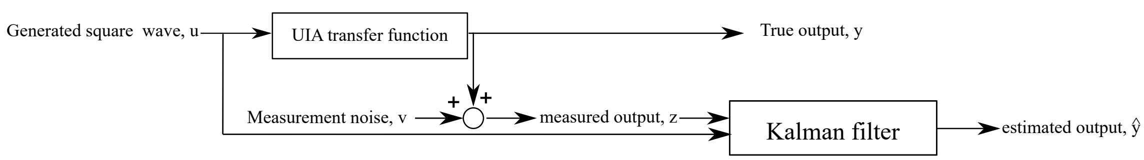

Fig. 3.5.: Block diagram for Kalman filter algorithm performance evaluation.

The Kalman filter estimation code was used to estimate the response,y of a square input, u, Figure 3.6, generated in Matlab 2016b to the UIA transfer function. A random noise signal, also generated in Matlab 2016b was added to the true response, y to simulate a noisy measured signal, z. The active input, u and measured noisy data, z were fed into the estimation code to evaluate the estimation performance. A positive outcome should be a close match of the estimated signal, $\hat{y}$ to the true response y, even though its being fed a noisy version, z, of the true response.

As shown in Figure 3.8 The estimated response is a close match to the true response, the difference between the true response and estimated response as well as the difference between true response and the noise introduced measured response is

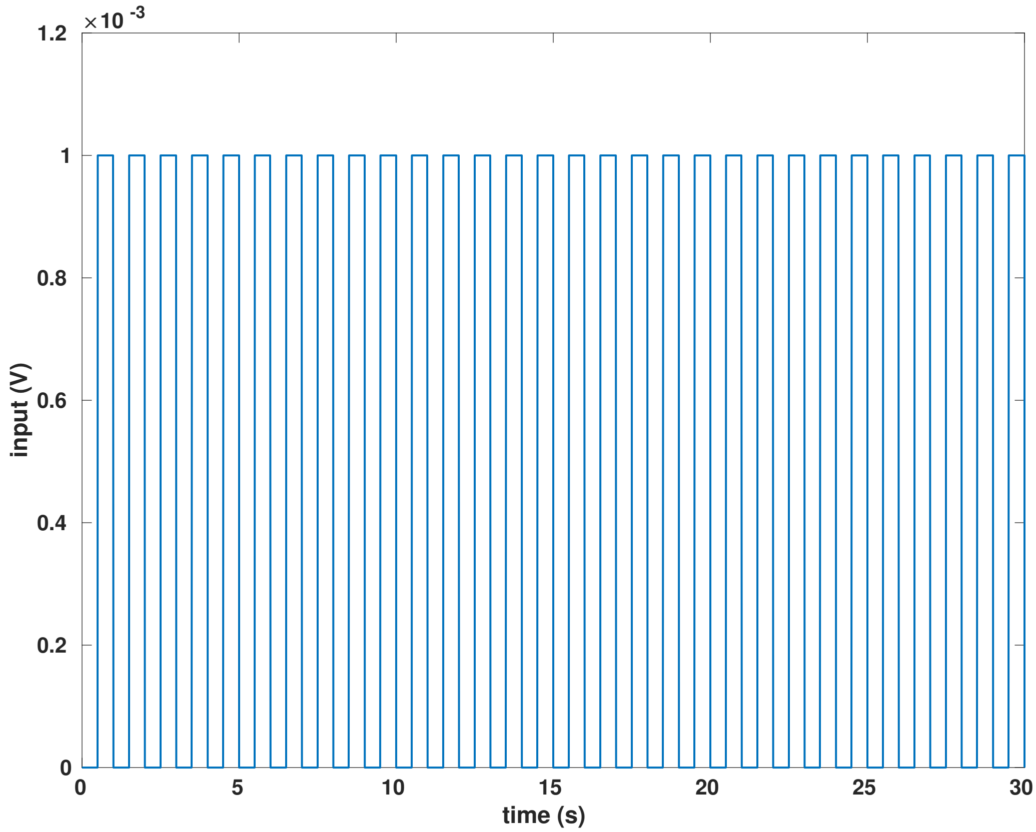

Fig. 3.6.: Square wave input signal for estimation code evaluation.

shown in Figure 3.9 which shows that the estimation algorithm was able to filter out most of the noise introduced in the measured data and estimate the actual response, the mean residual noise present in the measured data is 0.5 V where as the mean difference between y and ŷ is 0.0049 V.

It is noticeable from Figure 3.9 that at the very start of estimation the estimation error is very large. this is due to the blind initial estimate that is made prior to any knowledge about the system. The estimation algorithm adopts to the system model very fast and the error level comes down as it reaches steady state.

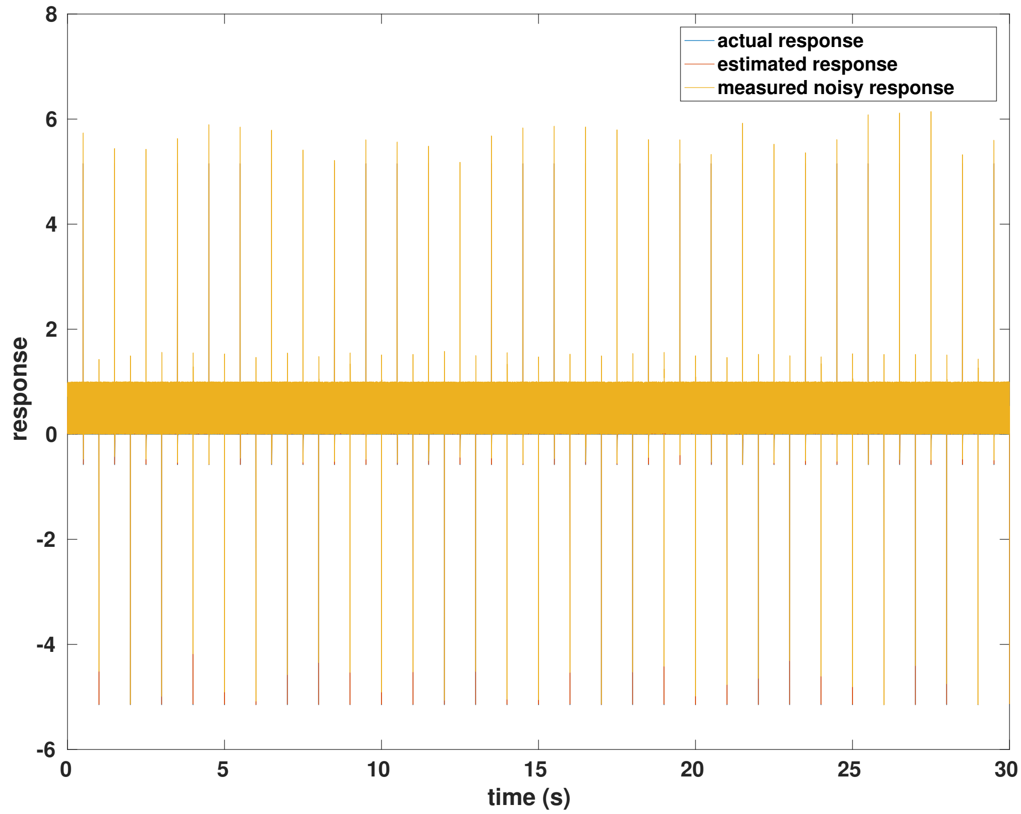

Fig. 3.7.: True response, estimated response and measured noisy response of the square wave to the input.

Even with the close estimation of response the estimated transfer function using the estimated response ŷ and the square wave input, u was not close to the actual transfer function that generated this response, UIA transfer function. Figure 3.11 and 3.12 show the significant error level at the low frequency region.

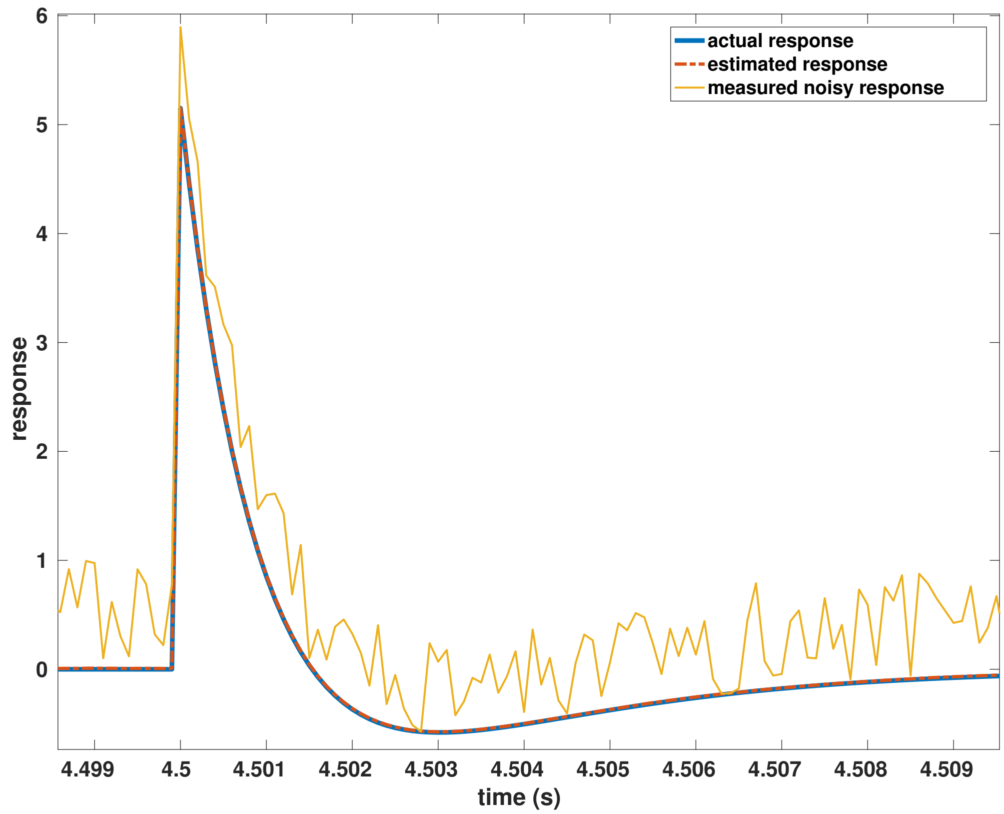

Fig. 3.8.: Zoomed in true response, estimated response and measured noisy response of the square wave to the input.

3.2.3 Transfer Function Split

To stabilize the transfer function estimation, UIA transfer function was split into two first order transfer functions reducing the number of pole and zero to be estimated to one. For UIA02,

$$\begin{aligned} TF &= \frac{5151(s+9.901)(s+8.344)}{(s+1000)(s+425.5)} \\ &= \frac{101(s+9.901)}{(s+1000)} \times \frac{51(s+8.344)}{(s+425.5)} \end{aligned} \tag{3.21}$$

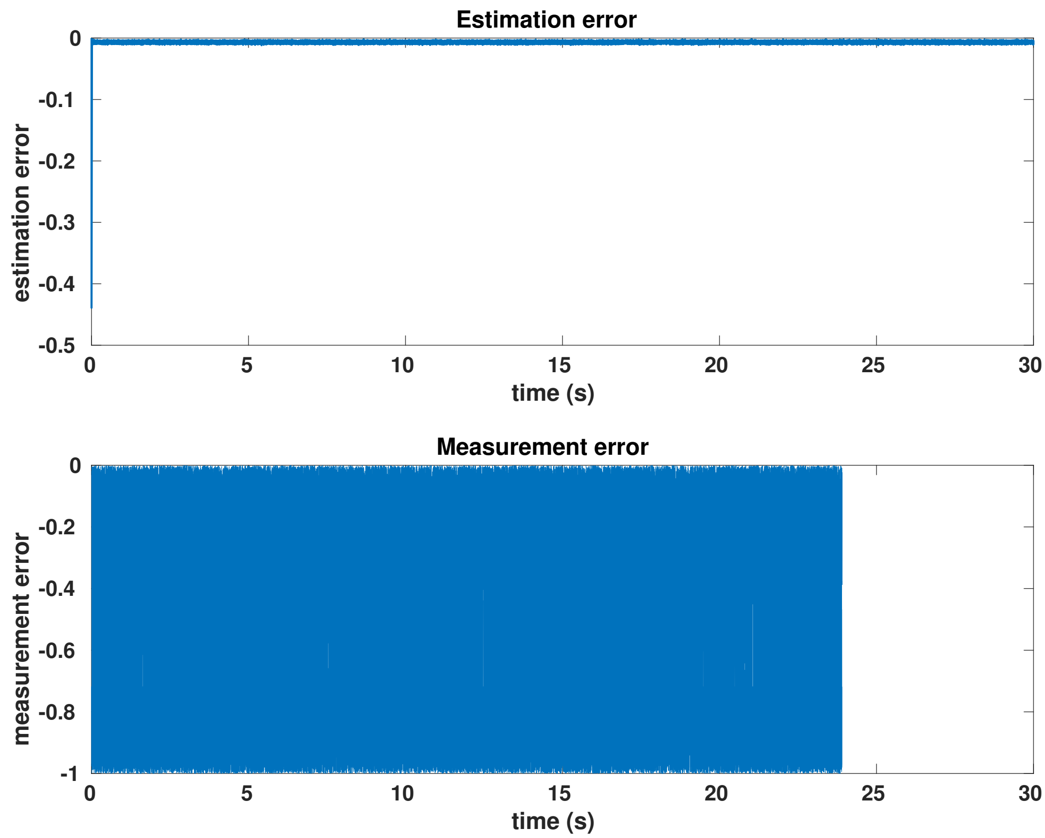

Fig. 3.9.: Estimation error (above) and measurement error (below) showing that the estimation algorithm successfully filtered out the injected noise.

With,

$$TF1 = \frac{101(s + 9.901)}{(s + 1000)} \tag{3.22}$$

$$TF2 = \frac{51(s + 8.344)}{(s + 425.5)} \tag{3.23}$$

Thus the estimation algorithm is used twice to estimate the reference responses at the first stage and the final stage. From these TF1 and TF2 are estimated and later combined to give the total transfer function estimate TF_{est}. This required us to

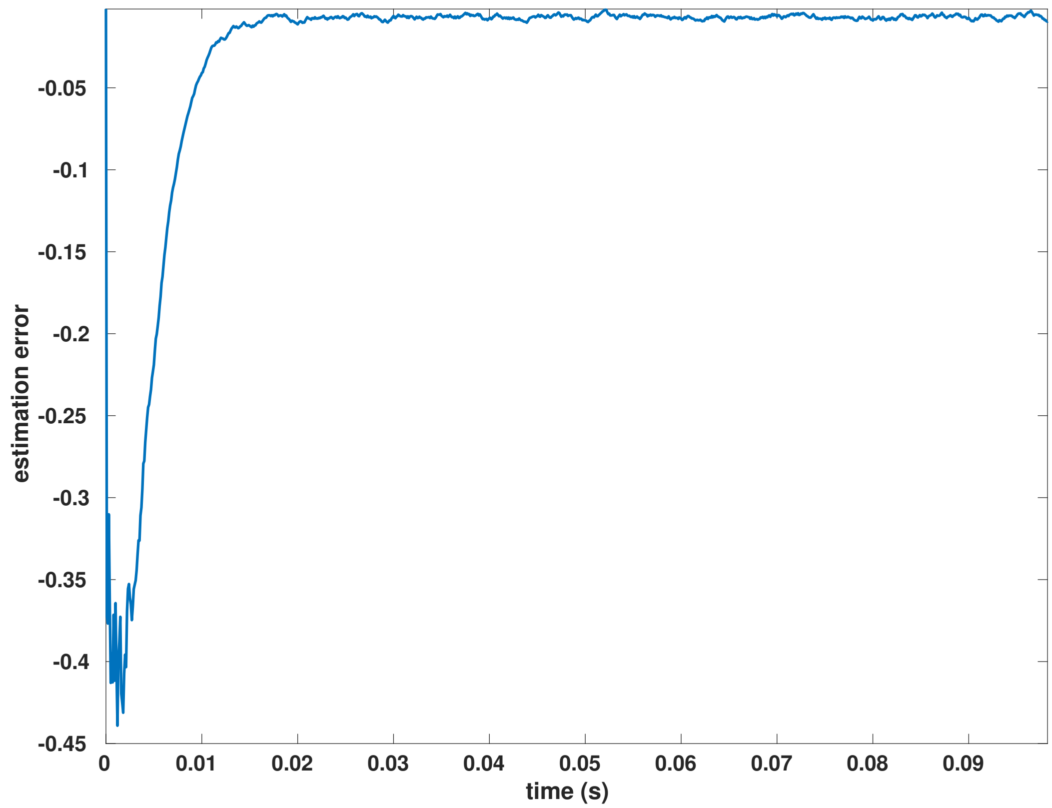

Fig. 3.10.: Transient estimation error at the start of estimation process.

take recording from the output of the first stage, $\mathbf{Z}1$ as well as the output of the final stage $\mathbf{Z}2$

The state space models for TF1 and TF2 are given by,

$$\mathbf{X}_k = 0.9792\mathbf{X}_{k-1} + 2\mathbf{U}_{k-1} \tag{3.24}$$

$$\mathbf{Y}_k = -1.031\mathbf{X}_k + 101\mathbf{U}_k \tag{3.25}$$

$$\mathbf{X}_k = 0.99912\mathbf{X}_{k-1} + 0.5\mathbf{U}_{k-1} \tag{3.26}$$

$$\mathbf{Y}_k = -0.8826\mathbf{X}_k + 51\mathbf{U}_k \tag{3.27}$$

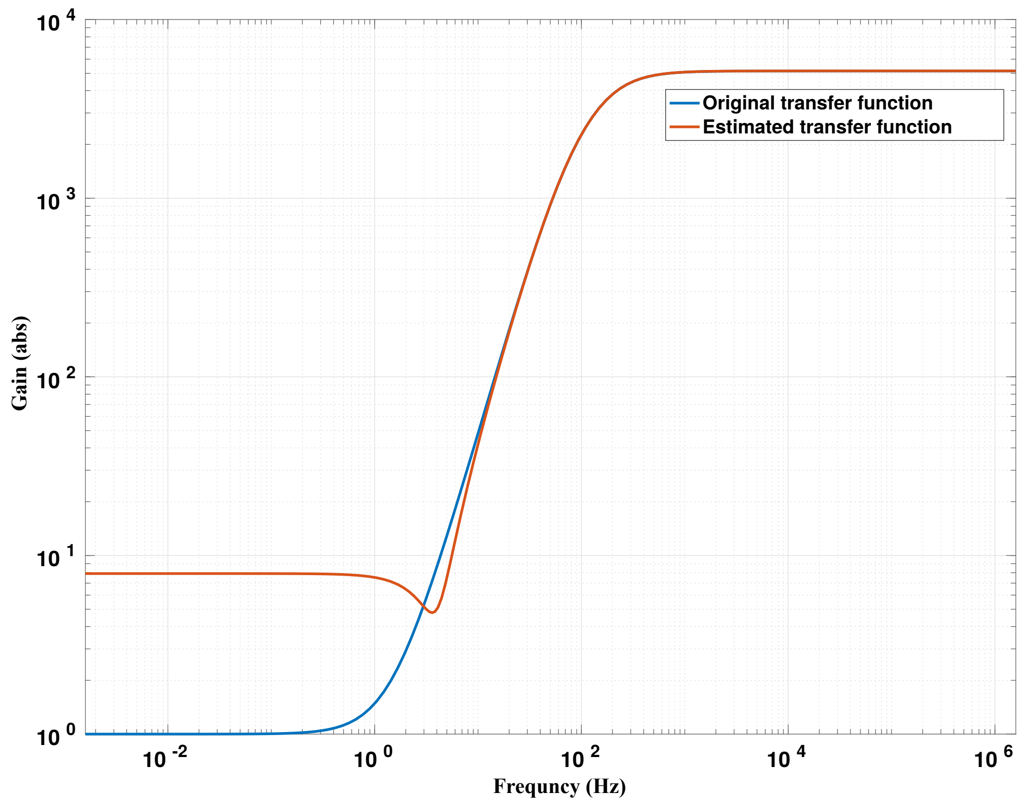

Fig. 3.11.: Unstable transfer function estimation even when reference response estimation performance was good.

And the estimated transfer functions are:

$$\mathrm{TF1}_{est} = \frac{\hat{\mathbf{Y}}1}{\mathbf{U}} \tag{3.28}$$

$$\mathrm{TF2}_{est} = \frac{\hat{\mathbf{Y}}2}{\hat{\mathbf{Y}}1} \tag{3.29}$$

$$\mathrm{TF}_{est} = \mathrm{TF1}_{est} \times \mathrm{TF2}_{est} \tag{3.30}$$

Since $\mathbf{Z}1$ is the output from the first stage of UIA it is also the input to the second stage and the estimated response, $\mathbf{Y}1$, of the reference, $\mathbf{U}$, at the output of first stage is the reference input of the second stage with its estimated response being $\mathbf{Y}2$. The split transfer function estimation process is summarized in the block diagram of Figure 3.13.

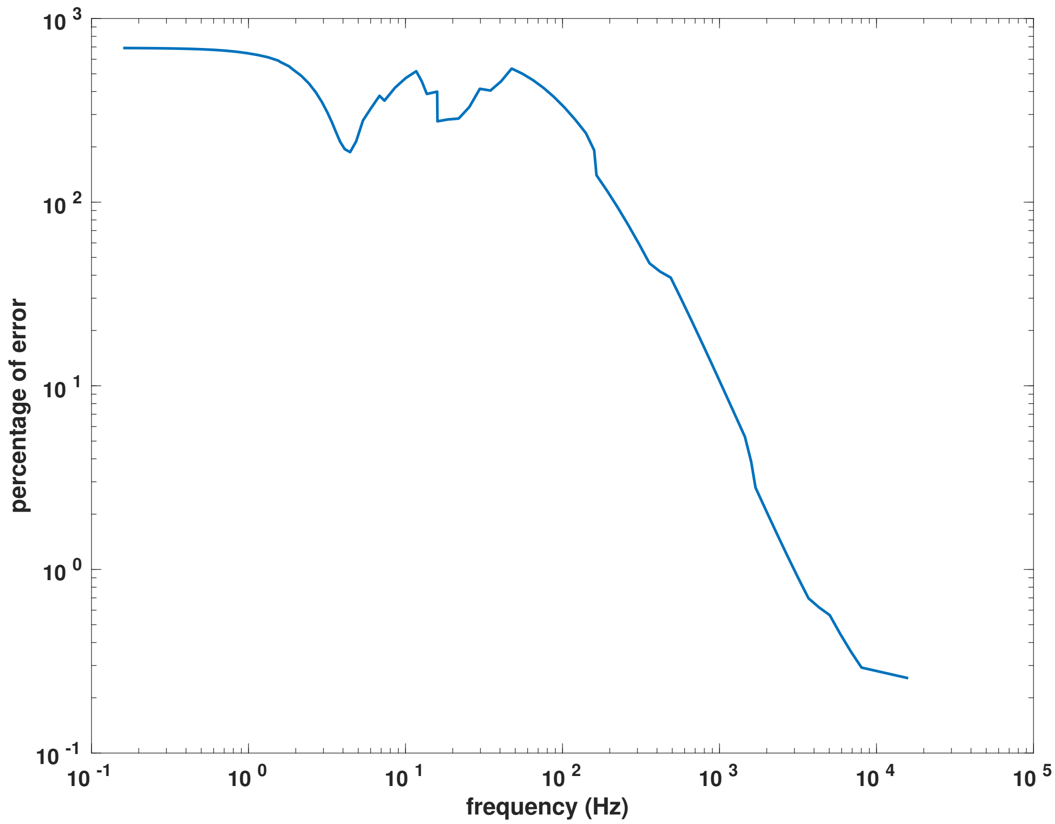

Fig. 3.12.: Estimation error.

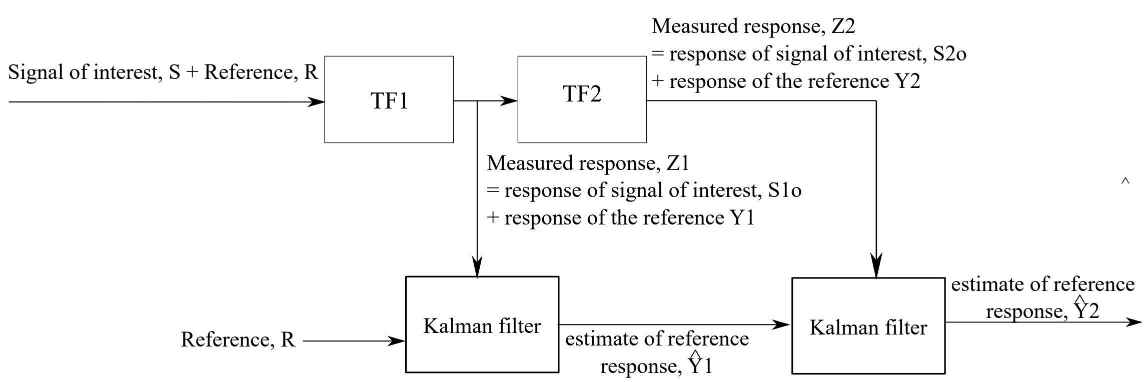

Fig. 3.13.: Block diagram for estimation process with split transfer function.

With the same square wave evaluation in Matlab The final transfer function estimation was a match to the original one, Figure 3.14.

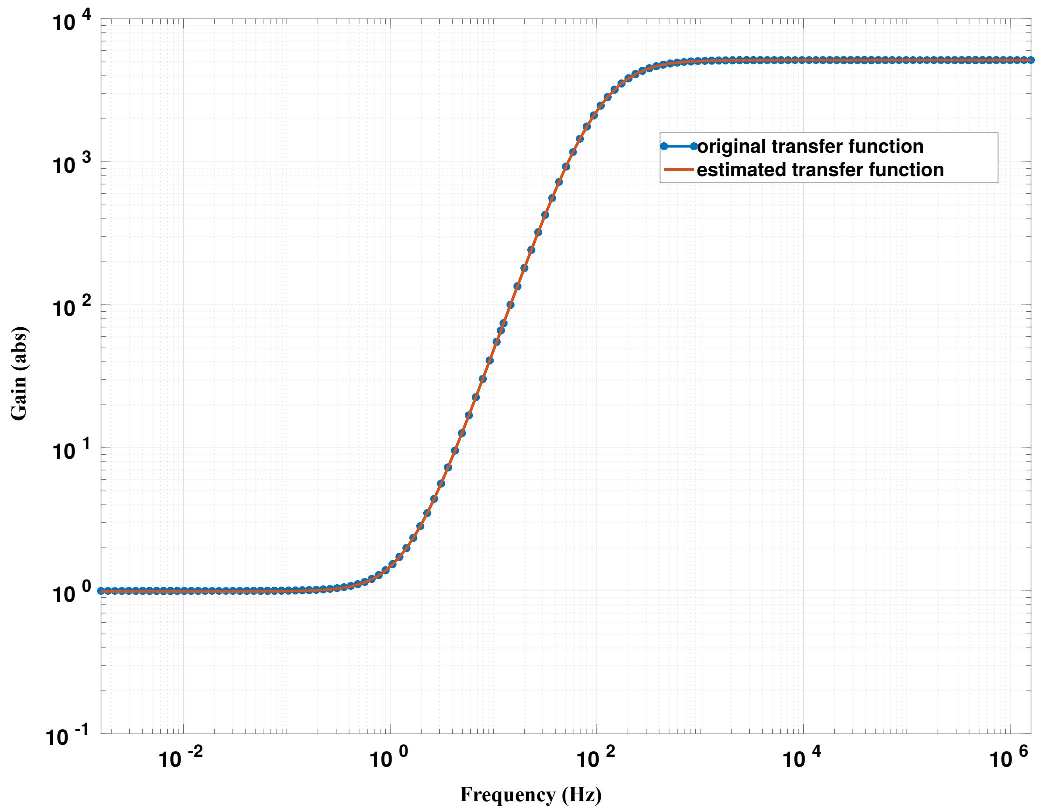

Fig. 3.14.: Transfer function estimation performance with split transfer function.

3.3 Use-Case: Using Digitally Generated Noise Input

Transfer function estimation using noise reference input was evaluated with UIA02 only. For broad spectrum transfer function estimation a noise signal is considered to be good, with it having equal response at all frequencies. But the initial trials suffered instability at lower frequency. Thus pink noise, which is low frequency spectrum noise was used as the reference in this use-case.

3.3.1 Noise Reference

Pink noise, shown in Figure 3.15 is a low frequency spectrum noise with power spectrum profile as shown in Figure 3.16. Pink noise input was digitally generated using Matlab 2016b and was injected into the second channel of UIA using NIDAQ (NI USB 6212) and LabVIEW 2014 as shown in block diagram 3.17. Output from the two stages was recorded and used to track the noise response.

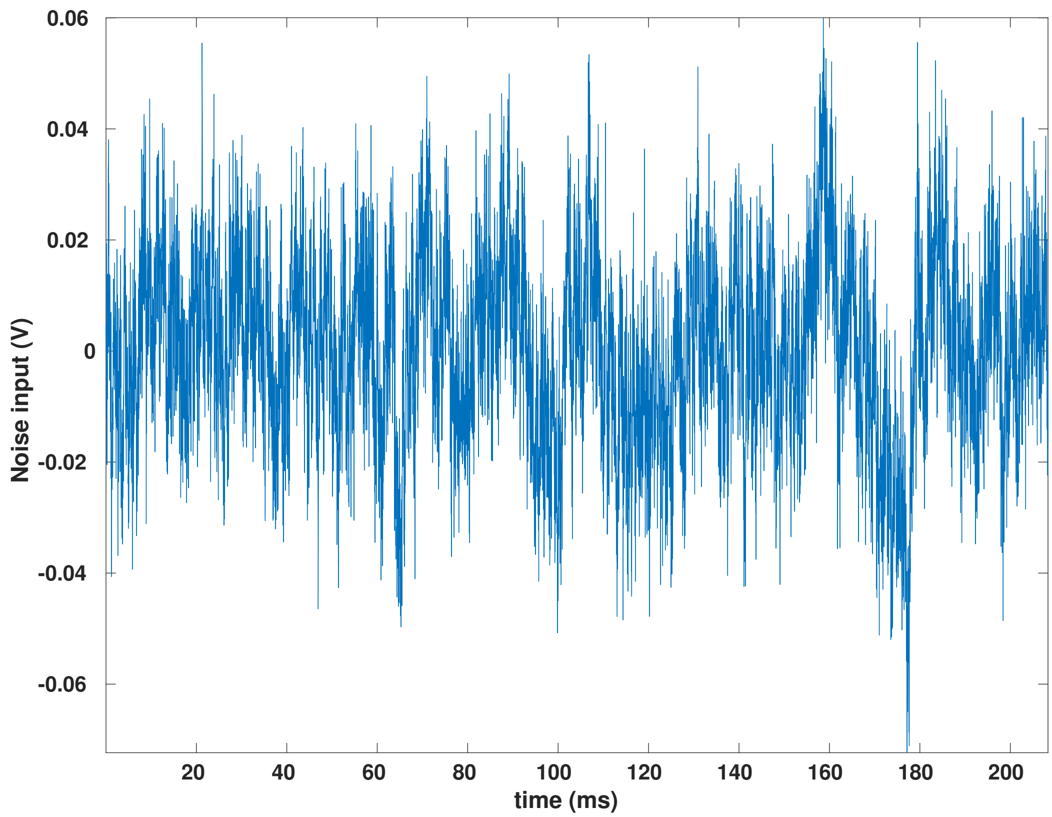

Fig. 3.15.: Pink noise reference input.

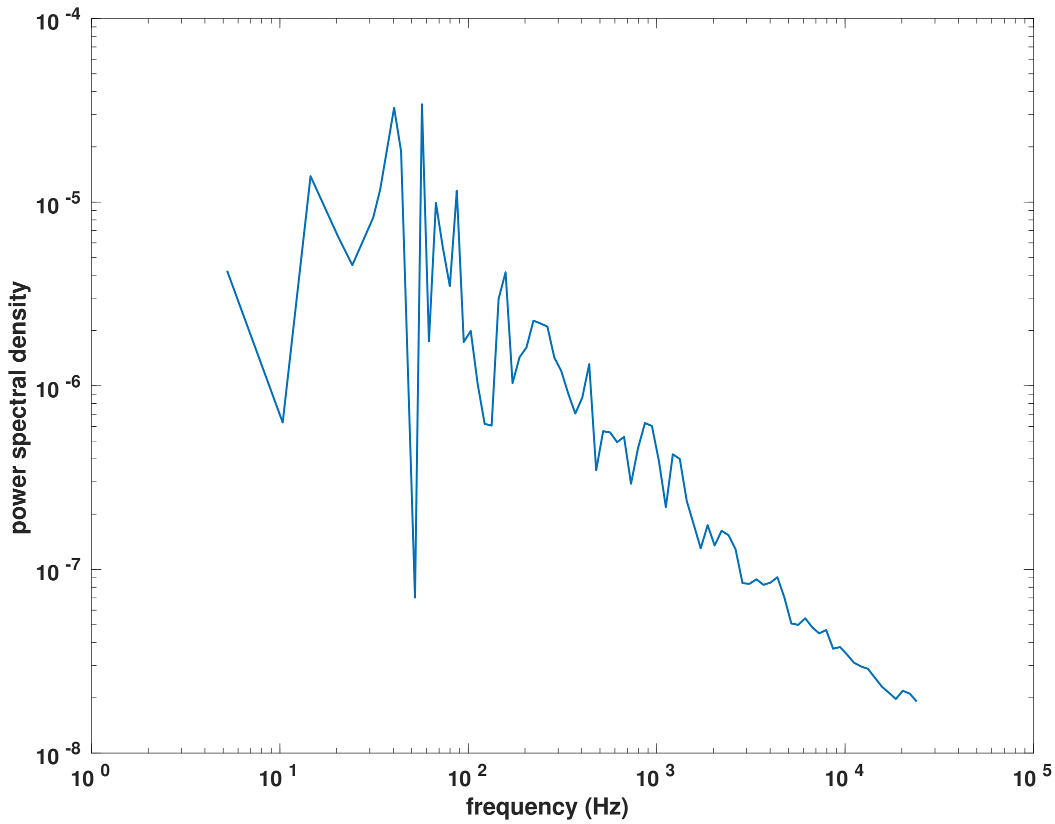

Fig. 3.16.: Pink noise power spectral density.

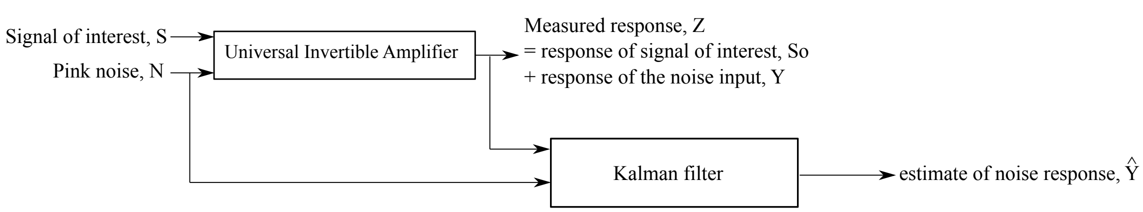

Fig. 3.17.: Block diagram for transfer function estimation using pink noise.

3.3.2 Estimated Transfer Function

The estimated transfer functions of the two stages from the tracked responses were,

$$TF1_{est} = \frac{100.9(s + 12.83)}{(s + 1003)} \tag{3.31}$$

$$TF2_{est} = \frac{51.16(s + 73.71)}{(s + 518.8)} \tag{3.32}$$

Giving the final result as Equation 3.33 and Figure 3.18

$$TF_{est} = \frac{5162.2(s + 12.83)(s + 73.71)}{(s + 1003)(s + 518.8)} \tag{3.33}$$

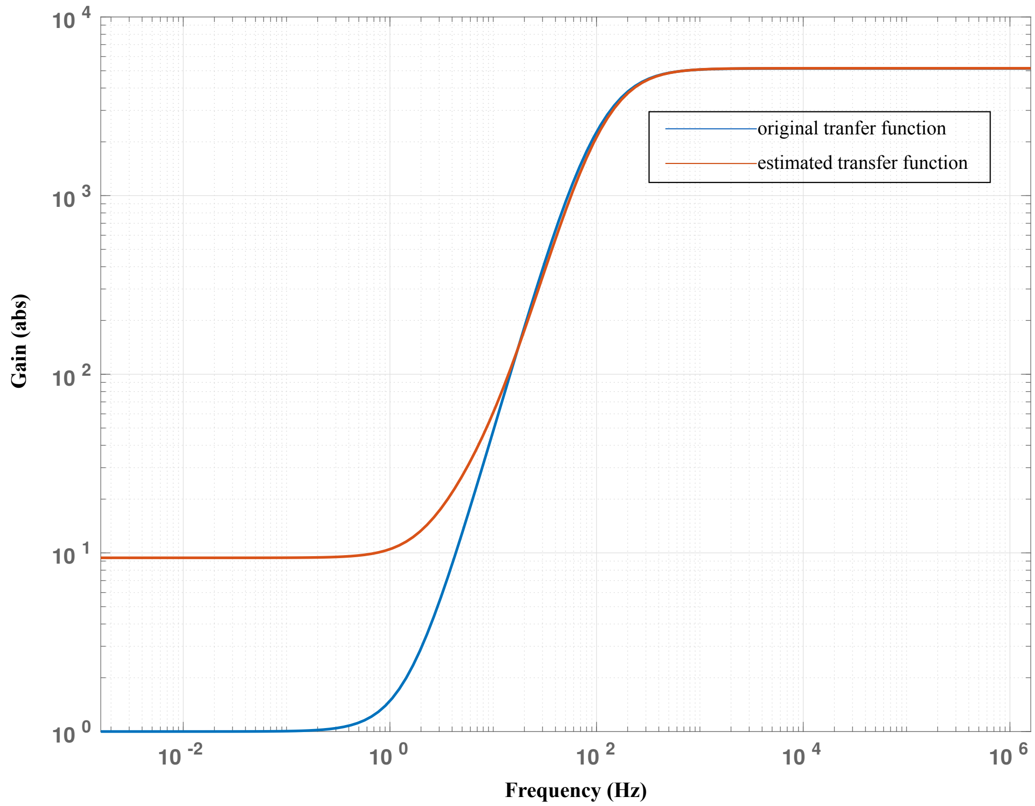

Fig. 3.18.: Transfer function estimation using noise input.

3.3.3 Estimation Error

Even with the split transfer function scheme estimation using noise reference still suffered significant error level, about 1000% in the low frequency range, DC-1Hz, Figure 3.19.

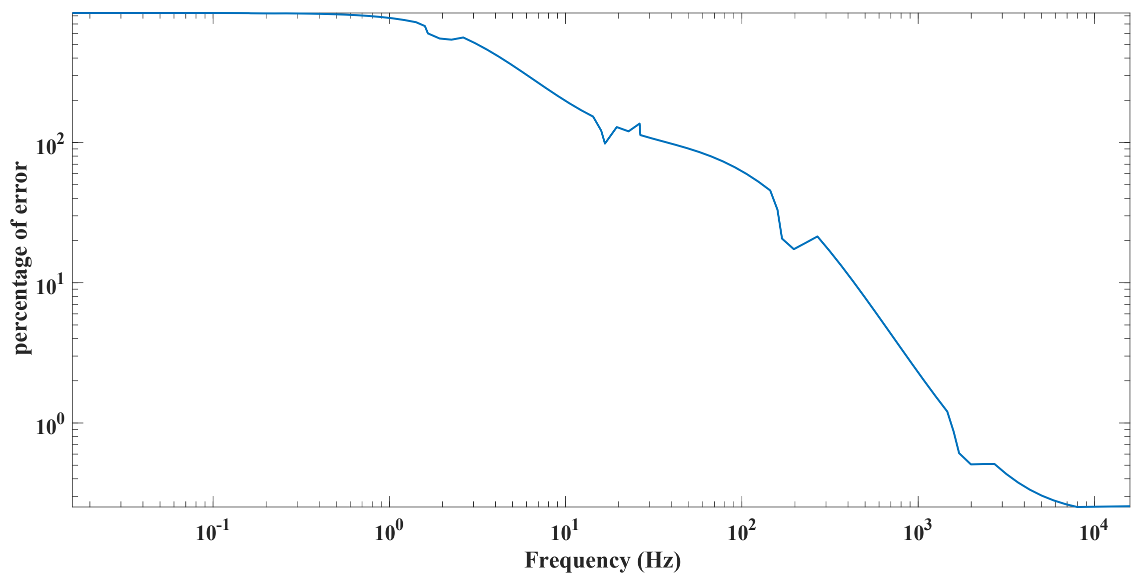

Fig. 3.19.: Estimation error for noise input estimation.

This was because of the smaller total sample numbers in the reference noise input. With larger signal the estimation performance would have improved. But the estimation performance using an inherent bio-signal noise produced far better results which inclined us towards exploring that route more.

4. CONTINUOUS CHARACTERIZATION USING BIO-SIGNAL

A common contaminant in bio-signal recordings is bio-signals originating from surrounding organ systems. In our cases, while recording from peripheral nerves, Electrocardiogram, ECG coupling happens more often than not acting as an in-band noise. However the ECG signal is something that is well-characterized [17] and is a very good candidate to be used as reference, which acts to our advantage. Instead of using an external reference signal, the pink noise, an inherent bio-signal noise could be used.

However to implement the idea a clean and simultaneous recording of the ECG contaminant input is required for the reference input. One way to do that was to record the ECG simultaneously while recording the signal of interest with a separate standard amplifier with a flat gain within the bandwidth of ECG. This simultaneous ECG input was used as the reference input to track its response mixed within the UIA output and estimate the transfer function using the reference and response.

4.1 Electrocardiogram, ECG

ECG is heart tissue activation signal, encompassing a bandwidth of roughly 0.2 Hz - 200 Hz [3]. The three major segments of the signal are the low-frequency P-wave, higher frequency QRS-complex followed by the low frequency T-wave. Its well defined [17] characteristics makes its response easier to follow and be used as reference.

4.2 ECG Response Estimation

The procedure for ECG response estimation is shown in Figure 4.1. ECG being the inherent bio-signal noise UIA did not require a second channel for reference injection. The reference signal seen at the input required for response estimation with Kalman filter was recorded with a second standard amplifier with a flat gain of 1000. The reference **U**, Figure 4.2, to the estimation algorithm was the output of the standard amplifier scaled down by the flat gain of the amplifier.

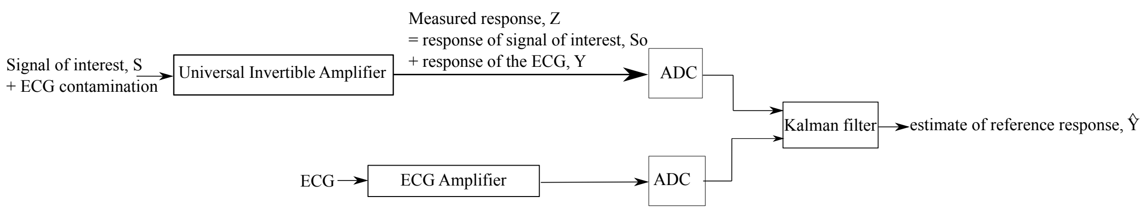

Fig. 4.1.: Transfer function estimation using inherent ECG contamination.

Using this reference, the ECG response was tracked from the mixed signal output, **Z** of UIA, Figure 4.3. Figure (ref) shows the estimated response, $\hat{\mathbf{Y}}$.

Data Collection

Same animal procedure as descried in Chapter 2 for Electrocardiogram data collection from Sprague Dawley rat vagus nerve was taken. All the procedure were conducted within the scope of protocol SC235R approved by IUPUI School of Science IACUC. TIME electrodes were used to collect spontaneous nerve activation data, signal of interest in this case, from the left vagus nerve in-vivo. Hypodermic needle (18 gauge) electrodes were used to record the simultaneous ECG reference from across the chest.

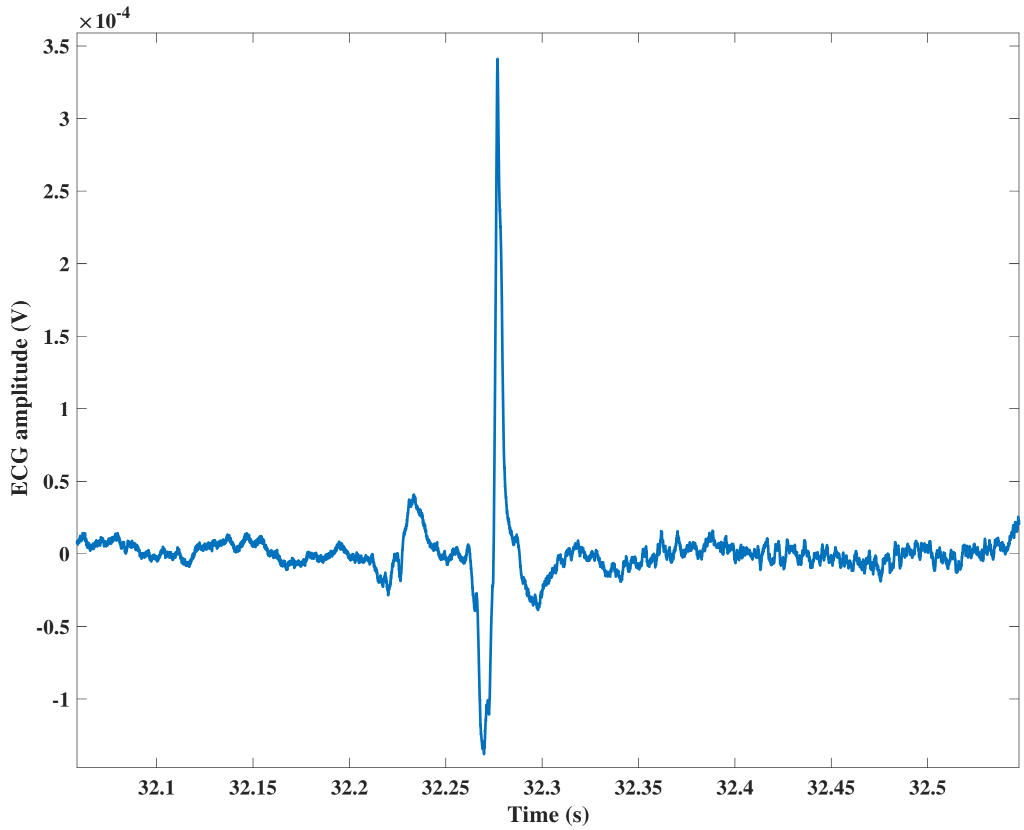

Fig. 4.2.: ECG reference recorded using standard amplifier.

4.3 Transfer Function Estimation

Transfer function estimate, TFest, Equation 4.1 was obtained from the estimated ECG response and the simultaneous reference record. Figure 4.5 shows a close match between the estimated transfer function and the original UIA transfer function with a percentage of error shown in Figure 4.6. The error level is still comparatively higher in the low frequency region but the mean percentage of error within 1Hz-100Hz being 10^{-2} it is fairly insignificant.

$$TF_{est} = \frac{5151(s+9.899)(s+8.349)}{(s+1000)(s+425.5)} \tag{4.1}$$

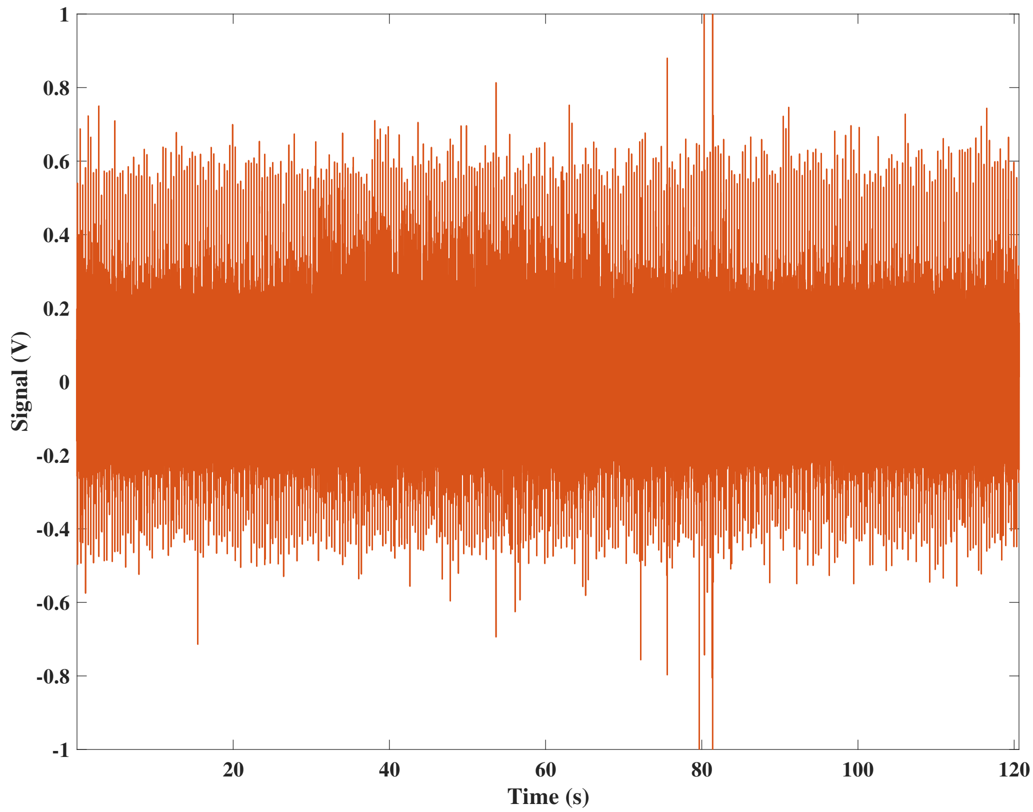

Fig. 4.3.: Mixed signal at the output of UIA.

Estimation error can be calculated using the equation of error propagation [15]. With dTF, dz1, dz2, dp1, dp2 being the difference in total transfer function, zero 1, zero 2, pole 1 and pole 2 the transfer function estimation error is given by 4.2,

$$\frac{dTF}{TF} = \frac{dz1}{z1} + \frac{dz2}{z2} + \frac{dp1}{p1} + \frac{dp2}{p2} \tag{4.2}$$

Successful transfer function estimation using ECG reference was reproduced 10 times with a mean estimation error of 0.09% calculated using Equation 4.2 which is considerably small making this a valid system characterization process.

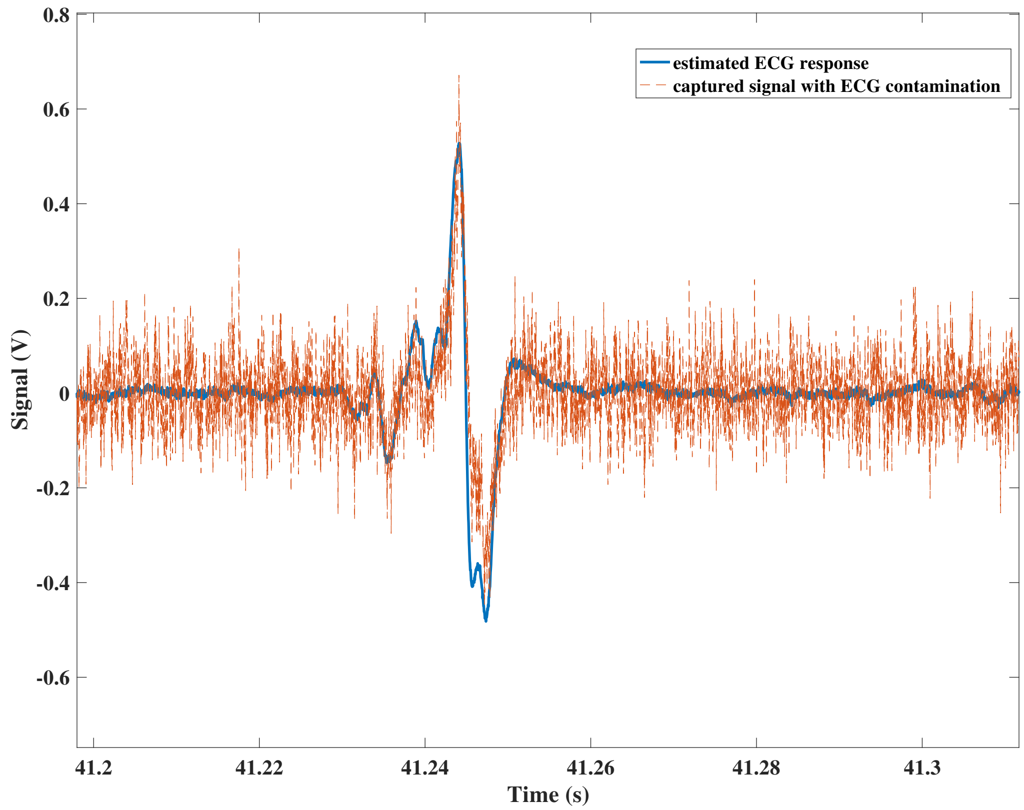

Fig. 4.4.: ECG response estimation in mixed signal.

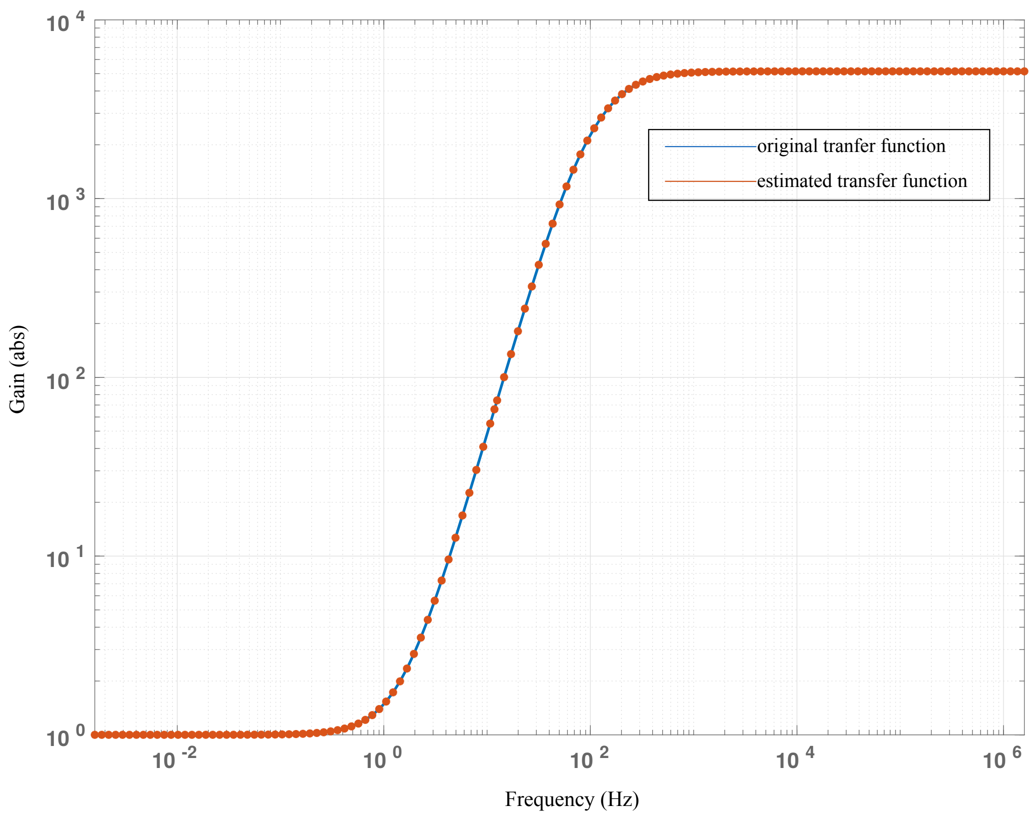

Fig. 4.5.: Transfer function estimation using ECG contamination.

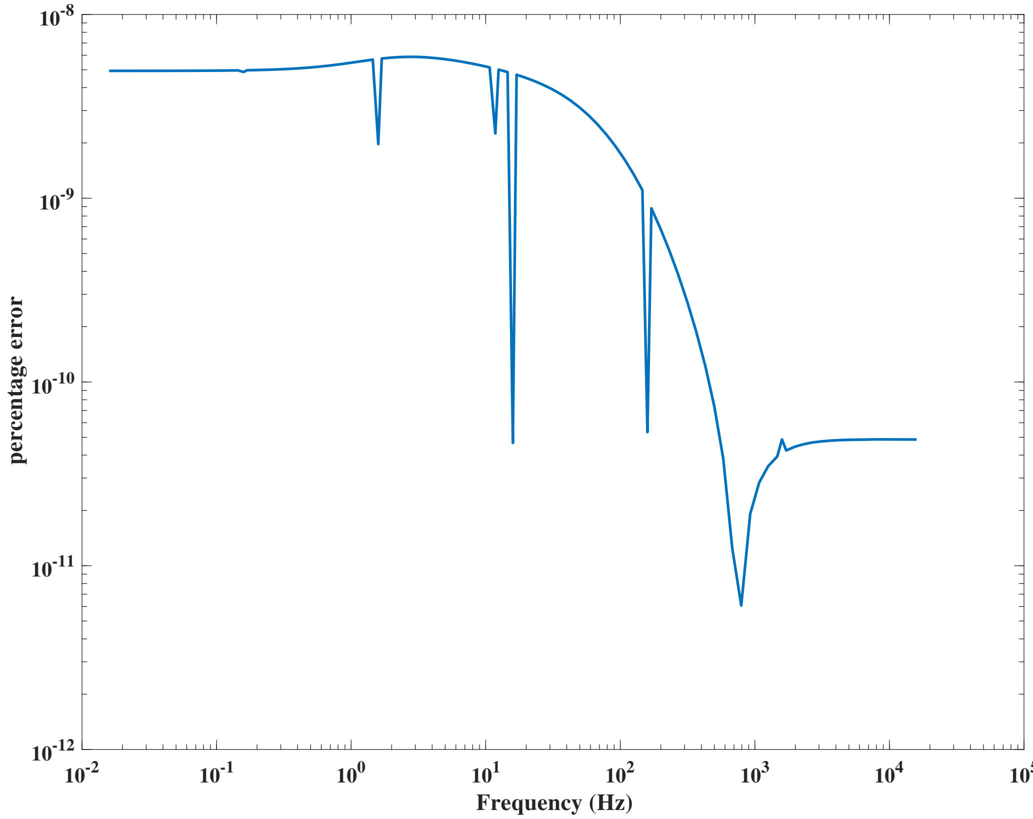

Fig. 4.6.: Transfer function estimation error using ECG reference.

5. SUMMARY AND CONCLUSION

The aims of this thesis work was to introduce a continuous characterization schema for higher order Universal Invertible Amplifier, UIA, with the objective of building high fidelity amplification system. A second order UIA was designed and several prototypes were built with that aim in mind and two different Use-Case Characterization techniques were tested with successful results.

Use-Case Characterization technique using external noise source was not as successful as the characterization scheme using inherent noise of the signal of interest, but there are still potential ways of making the technique better. As we obtained better results with using inherent noise source we stopped pursuing those techniques. However, for systems for which an external noise reference will be suitable this technique can be easily tried out.

For Use-Case Characterization using inherent noise of the system we used ECG cross contamination which is a very well-defined reference and can be captured using standard amplification systems for collection of a simultaneous reference signal. Not all systems have such a well-defined noise contamination and it can be difficult, if not impossible, to characterize the inherent noise as well as its response to the amplifier-filter chain system that needs to be characterized. Thus a future focus for this work can potentially be tracking inherent noise of a system without a reference, but just from the known *apriori* system definition.

As for the Universal Invertible Amplifier system, a complete system with the low noise headstage in the form of a product is the immediate future goal. We believe it can be a useful application in the biomedical research world and with more improvements in time i the diagnostic medicine as well. However the Characterization of system using its inherent noise may have far reaching potential applications, with any unstable longterm use system.

LIST OF REFERENCES

LIST OF REFERENCES

[1] K. Mauser, "A Digitally Invertible Universal Amplifier for Recording and Processing of Bioelectric Signals," Thesis, Purdue University.

[2] K. Yoshida, K. Mauser, and J. Stavnshoj, "Digitally invertible universal amplifier for recording and processing bioelectric signals,US Patent #9,622,672b2, Issued 18.4.2017."

[3] R. Sherman_Gold, "The Axon Guide for Electrophysiology & Biophysics Laboratory Technique."

[4] A. B. Clark, ""Electrical picture-transmitting system'," Patent, Nov., 1928.

[5] "INA111 datasheet." [Online]. Available: http://www.ti.com/lit/ds/symlink/ina111.pdf

[6] "OP27 datasheet." [Online]. Available: http://www.analog.com/media/en/technical-documentation/data-sheets/OP27.pdf

[7] M. S. Grewal and A. P. Andrews, *Kalman filtering: theory and practice using MATLAB*, 3rd ed. Hoboken, N.J: Wiley, 2008, oCLC: ocn191758403.

[8] R. E. Kalman, "A New Approach to Linear Filtering and Prediction Problems," *Journal of Basic Engineering*, vol. 82, no. 1, pp. 35–45, Mar. 1960. [Online]. Available: http://dx.doi.org/10.1115/1.3662552

[9] R. G. Brown, *Introduction to random signal analysis and Kalman filtering*. New York: Wiley, 1983.

[10] R. A. DeCarlo, *Linear systems: a state variable approach with numerical implementation*. Englewood Cliffs, N.J: Prentice Hall, 1989.

[11] W. L. Brogan, *Modern control theory*, 3rd ed. Englewood Cliffs, N.J: Prentice Hall, 1991.

[12] G. Welch and G. Bishop, "An Introduction to the Kalman Filter," Jul. 2006.

[13] "Noise Analysis in Operational Amplifier Circuits." Texus Instruments, Application Report.

[14] "Low Noise, Low-Distortion Instrumentation Ampplifier Replacement for SSM2017 (Rev. C) - ina217.pdf." [Online]. Available: http://www.ti.com/lit/ds/symlink/ina217.pdf

[15] J. R. Taylor, *An introduction to error analysis: the study of uncertainties in physical measurements*, 2nd ed. Sausalito, Calif: University Science Books, 1997.

[16] P. S. Maybeck, *Stochastic models, estimation and control*, ser. Mathematics in science and engineering. New York: Academic Press, 1979, no. v. 141.

[17] S. Grimnes and . G. Martinsen, *Bioimpedance and bioelectricity basics*, 2nd ed. London: Academic Press, 2008, oCLC: 845287071.